
Adaptation of DOAS algorithm directly on interferograms acquired with an interferometric hyperspectral camera

Yann Bourdin

Grenoble INP - Phelma, UGA

Internship carried out in:

Institut des Géosciences de l'Environnement (IGE), Grenoble, France

under the supervision of:

Didier Voisin (IGE)

didier.voisin@univ-grenoble-alpes.fr

Aneline Dolet (GIPSA-lab)

aneline.dolet@gipsa-lab.grenoble-inp.fr

Internship Report – Jun - Aug 2021

Ce rapport s'intéresse à un prototype de spectromètre imageur à transformée de Fourier abordé sous l'angle du traitement du signal, dans le but de mesurer des densités de colonne de gaz atmosphériques. Nous proposons une méthode s'appuyant sur une modélisation optique de l'instrument, adaptée d'une technique existante, mais qui s'applique sur des interférogrammes au lieu de spectres. Les résultats sont prometteurs mais d'autres développements sont nécessaires afin de valider ces derniers.

This report focuses on a prototype of Fourier transform imaging spectrometer approached from a signal processing perspective, with the goal of retrieving column densities of atmospheric gases. We propose a method relying on an optical modeling of the instrument, adapted from an existing technique, but that applies on interferograms instead of spectra. The results are promising but more developments are needed in order to validate the latter.

Contents

Introduction	1
Context of the project	1
1 Differential Optical Absorption Spectroscopy	2
1.1 Absorption spectroscopy	2
1.2 The DOAS principle	3
1.3 Application to atmospheric measurements	4
1.4 Focus on retrieving column densities of NO ₂	5
2 ImSPOC Acquisition Model	5
2.1 Sensor principle	5
2.2 Principles of Fabry-Pérot interferometry	7
2.3 Modeling the sensor	9
3 Python Module	11
3.1 Raw data processing	11
3.2 Interferogram extraction	12
4 Measurements	12
5 Estimation of Column Densities	14
5.1 Beer-Lambert on interferograms	14
5.2 Gas correlation	15
5.3 AMF calculation	16
6 Results	16
6.1 Simulation and noise considerations	16
6.2 Results	19
Conclusion	21
Appendix	22
Python notebook for the processing of zenith scattered light data	22

List of Figures

1	Sketch of direct light observation geometries.	5
2	Absorption cross-section spectrum of NO ₂ : $\alpha_{NO_2}(\sigma)$.	6
3	Differential absorption cross-section spectrum of NO ₂ in the bandwidth of the interferential filter : $\widetilde{\alpha_{NO_2}}(\sigma)$.	6
4	Scheme of the ImSPOC prototype with its components.	7
5	Transfer function of the interferential filter.	8
6	Raw data obtained with ImSPOC.	8
7	Scheme of a Fabry-Pérot cavity.	9
8	Filtering effect of a Fabry-Pérot cavity of thickness $\delta = 2\mu m$.	10
9	Acquisition scheme.	13
10	Capture setups for zenith and direct observations.	13
11	Calculated AMF of zenith scattered light with Sarkissian's model, shown in function of the solar zenith angle and in function of time.	17
12	Relative error on the estimated vertical column density on simulated interferograms in function of the signal-to-noise ratio (SNR).	18
13	NO ₂ correlation (or covariance) in function of time for zenith scattered light measurements.	19
14	NO ₂ correlation (or covariance) in function of time for zenith scattered light measurements at morning and at evening.	19
15	NO ₂ correlation (or covariance) in function of the calculated AMF for zenith scattered light.	20
16	NO ₂ correlation (or covariance) in function of the geometrical AMF for direct light.	20

Acronyms

ADU Analog-to-digital unit.

AMF Air Mass Factor.

CCD Charge-coupled device.

DOAS Differential Optical Absorption Spectroscopy.

FITS Flexible Image Transport System.

FPI Fabry-Pérot Interferometer.

GIPSA-lab Grenoble Images Parole Signal Automatique / Grenoble images speech signal and control laboratory.

IGE Institut des Géosciences de l'Environnement / Institute for geosciences and environmental research.

ImSPOC Image Spectrometer on Chip.

IPAG Institut de Planétologie et d'Astrophysique de Grenoble / Institute for planetary sciences and astrophysics.

OPD Optical Path Difference.

SCD Slant Column Density.

SNR Signal-to-noise ratio.

UGA Université Grenoble-Alpes.

VCD Vertical Column Density.

Nomenclature

$\alpha(\sigma)$ Absorption cross-section at wavenumber σ ($cm^2/\text{molecules}$)

\cdot_j Relative to gas j

$\Delta \cdot$ Difference between two points

δ Optical path difference (OPD) (m)

λ Wavelength (m)

$\langle \cdot \rangle$ Low-pass filtered component

$\mathcal{F}[\cdot]$ Fourier transform

$\mathcal{T}(\sigma)$ Transfer function

$\bar{\cdot}$ Mean value

σ Wavenumber (m^{-1})

$\tilde{\cdot}$ High-pass filtered component

$I(\delta)$ Interferogram – radiance at OPD δ

$I(\sigma)$ Spectral light intensity (or radiance) ($W.sr^{-1}.m^{-2}.m$)

s Slant column density (SCD) (molecules/ cm^2)

$\text{Cov}(x, y) = \int (x - \bar{x})(y - \bar{y})$ – Covariance

$\text{Re}\{\cdot\}$ Real part

$\text{Var}(\cdot) = \text{Cov}(\cdot, \cdot)$ – Variance

Introduction

Teledetection of atmospheric gases is more than a century old. It has been made possible mainly with absorption spectroscopy, the study of the absorption of electromagnetic radiation by matter. Initially used from the ground, it has been applied from space since the first weather satellites in the 1970s, enabling access to ever more detailed information about the Earth's surface and atmosphere. This technology is now a key element of our observation strategies for environmental monitoring, and is a reasonable option for providing constraints on pollutant emissions for air quality monitoring in the coming decades. A modern and well-established method of measuring the column densities of trace gases in the atmosphere is named Differential Optical Absorption Spectroscopy (DOAS).

In this report we focus on a miniature hyperspectral Fourier transform camera, developed at the Université Grenoble Alpes by IPAG (Institute for Planetary sciences and Astrophysics). This camera is known under the patent ImSPOC (Image Spectrometer on Chip), and is based on an array of Fabry-Perot interferometers mounted over a high-sensitivity CCD imaging system (a matrix of photodiodes). It produces a matrix of images which can be recombined in order to form a single hyperspectral image of the observed scene. Being the size of a matchbox, it could become a base brick for nano-satellites, drones, or ground-based measure platforms.

The DOAS method fundamentally implies measuring light spectra. However, the spectral information captured by ImSPOC is not directly spectra, but partial interferograms with non-uniform sampling. Thus, the measurements must undergo a signal processing step in order to provide usable data for applications.

The objective of the internship has been to explore the adaptation of the DOAS method directly on interferograms instead of spectra. In particular, the goal has been to evaluate the concentration of nitrogen dioxyde (NO_2) in the atmosphere, from data acquired with an interferential filter, targeting this specific gas, mounted on an ImSPOC prototype.

First, we will present the DOAS technique adapted to our context, then we will tackle the optical modeling of the ImSPOC sensor. We will see how the data is processed before turning on to the way we did our measurements. Finally we present our method enabling us to retrieve column densities and show the obtained results with this method.

Context of the project

The Institute for Geosciences and Environmental research (IGE) is a public research laboratory in Earth and Environmental Sciences, located on the university campus of Grenoble, in France. It is a joint research unit supervised by CNRS (Centre National de la Recherche Scientifique), IRD (Institut de Recherche pour le Développement), UGA (Université Grenoble-Alpes), and Grenoble INP.

This project took place within the Atmospheric Chemistry team, which aims at identifying the sources, sinks and transformation mechanisms of chemical species generated by human activities; and in particular, determining their impact on climate, air quality

and snow-covered ecosystems.

The ImSPOC prototype is actively in development in collaboration between 3 laboratories: IPAG, GIPSA-Lab (Grenoble Images Speech Signal and Control) and IGE.

1 Differential Optical Absorption Spectroscopy

Platt and Stutz [1] is the reference book of this technique.

1.1 Absorption spectroscopy

Absorption spectroscopy takes its root in the Beer-Lambert's law which, in a formulation suitable for the analysis of gaseous or liquid absorbers, can be written as:

$$I(\sigma) = I_0(\sigma) \cdot \exp(-\alpha(\sigma) \rho L) \quad (1.1)$$

where $I_0(\sigma)$ is the spectral intensity of an emitted light beam, and $I(\sigma)$ is the intensity of the beam after passing through a layer of thickness L , where the absorber is present at a uniform concentration of ρ . $\alpha(\sigma)$ denotes the absorption cross-section of the absorber at wavenumber σ . The wavenumber is defined as the inverse of wavelength, i.e. $\sigma = \frac{1}{\lambda}$.

We may define the **optical density** of an absorber as:

$$D = \ln \left(\frac{I_0(\sigma)}{I(\sigma)} \right) = \alpha(\sigma) \rho L \quad (1.2)$$

The absorption cross-section spectrum of a species is unique, like a fingerprint, and can be calculated or measured. Once we know the light path L and D is measured, the concentration can be obtained by evaluating $\rho = D / (\alpha(\sigma) \cdot L)$.

However in the atmosphere, several effects can cause the extinction of a light ray, such as absorption due to certain gases, Rayleigh and Mie scattering, and turbulence. Thus Beer-Lambert's law (1.1) can be expanded to:

$$\begin{aligned} I(\sigma) &= I_0(\sigma) \cdot \exp \left[- \int_{\text{light path}} \left(\sum_j (\alpha_j(\sigma) \cdot \rho_j(l)) + \varepsilon_R(\sigma, l) + \varepsilon_M(\sigma, l) \right) dl \right] \cdot A(\sigma) \\ &= I_0(\sigma) \cdot \exp \left[- \sum_j \alpha_j(\sigma) \cdot s_j \right] \cdot \exp \left[\int_{\text{light path}} \varepsilon_R(\sigma, l) + \varepsilon_M(\sigma, l) dl \right] \cdot A(\sigma) \end{aligned} \quad (1.3)$$

where

- $\alpha_j(\sigma)$ (resp. ρ_j) is the absorption cross section at wavenumber σ (resp. average concentration over light path) of gas j

- s_j is the **column density** of gas j. It is the integral of its concentration over the light path: $s_j = \int \rho_j(l)dl$.
- $\varepsilon_R(\sigma, l)$ and $\varepsilon_M(\sigma, l)$ are respectively Rayleigh and Mie extinction effects at wavenumber σ and position l on the light path.
- $A(\sigma)$ summarizes turbulence and instrumental effects.

In the case of multiple light rays, and so multiple light paths, their contributions have to be summed.

1.2 The DOAS principle

Using equation (1.3) to measure a specific trace gas concentration, it would be necessary to quantify every factor influencing the light extinction. One could do so by removing the absorber from the light path, it is however impossible to do in the atmosphere.

The fundamental idea of Differential Optical Absorption Spectroscopy (DOAS) is to notice that most extinction effects present smooth, low frequency spectral characteristics, while trace gases may show high frequency spectral content in certain wavenumber intervals.

$$\alpha(\sigma) = \langle \alpha \rangle(\sigma) + \tilde{\alpha}(\sigma) \quad (1.4)$$

where $\langle \alpha \rangle(\sigma)$ is the low-frequency general slope of the absorption cross section with respect to wavenumber σ ; $\tilde{\alpha}(\sigma)$ is the residual high-frequency component. The cut-off frequency between both components should be adjusted depending on the gas. The separation between these components for NO₂ is shown in figures 2 and 3.

Inserting (1.4) into (1.3), we obtain:

$$I(\sigma) = I'_0(\sigma) \cdot \exp \left(\sum_j (\tilde{\alpha}_j(\sigma) \cdot s_j) \right) \quad (1.5)$$

where $I'_0(\sigma)$ is the intensity spectrum in absence of differential absorption, summarizing all other extinction effects.

The resulting optical density is:

$$D' = \ln \frac{I'_0}{I} = \sum_j \tilde{\alpha}_j(\sigma) \cdot s_j \quad (1.6)$$

Now the optical density D' is only the sum of the optical densities of the absorbers. However, in many cases we do not have access to the spectrum $I'_0(\sigma)$. Moreover, what we really measure when doing DOAS is not $I(\sigma)$ but $I(\sigma) \times A(\sigma)$, where A is the instrumental function, and this function is a factor in I'_0 . Instead of relying on I'_0 , we can use a reference spectrum $I_1(\sigma)$ taken with the same instrument as $I(\sigma)$ so that the instrumental function is cancelled out, and what we measure are differential columns:

$$\Delta D' = \ln \frac{I^A(\sigma)}{I^B(\sigma)} = \ln I_0'^A - \ln I_0'^B + \sum_j \widetilde{\alpha}_j(\sigma) \cdot \Delta s_j \quad (1.7)$$

where $\Delta s_j = s_j^B - s_j^A$

$I_0'(\delta)$ being essentially low-frequency, by filtering $\Delta D'$ we can obtain a differential optical density equal to the differential optical densities of trace gases:

$$\widetilde{\Delta D'} = \ln \widetilde{\frac{I^A(\sigma)}{I^B(\sigma)}} = \sum_j \widetilde{\alpha}_j(\sigma) \cdot \Delta s_j \quad (1.8)$$

Finally, we apply a curve-fitting method to the equation $y = f(\sigma, \Delta s_1, \dots, \Delta s_J)$ (with $y = \ln \frac{I^A(\sigma)}{I^B(\sigma)}$ and $f(\sigma, \Delta s_1, \dots, \Delta s_J) = \sum_j \widetilde{\alpha}_j(\sigma) \cdot \Delta s_j$) in order to estimate all s_j . Another variant is to estimate successively the s_j , first we fit y with $\widetilde{\alpha}_1(\sigma) \cdot \Delta s_1$, we subtract the fitted curve to obtain the residual, then we do the same on the residual for $\widetilde{\alpha}_2(\sigma) \cdot \Delta s_2$, etc... (the gases being ordered by decreasing optical density).

1.3 Application to atmospheric measurements

When measuring optical densities of atmospheric gases, the incident light spectrum I_0 is emitted by the sun. The optical density of the measured spectrum I is the result of multiple light rays that travelled through the atmosphere with different paths and extinction processes. In order to retrieve the column density of a gas, and so its concentration, we have to introduce the Slant Column Density (**SCD**), the Vertical Column Density (**VCD**), and the Air Mass Factor (**AMF**). The VCD is the column density corresponding to a vertical direct light ray through the atmosphere, with a solar zenith angle of 0° . The SCD is the column density s_j that we measure. The AMF is the ratio of the SCD over the VCD:

$$\mathbf{AMF} = \frac{\text{SCD}}{\text{VCD}} \quad (1.9)$$

Figure 1 explicits the variation of the air mass factor with the solar zenith angle, for a direct ray. As the angle increases, the light traverses a longer, ‘slanted’ path, through the gas layer.

In order to retrieve the VCD from the SCD, we must calculate the AMF beforehand (see section 5.3) or possibly measure it. Keep in mind the SCD of a gas j corresponds to the s_j coefficient of (1.8). Suppose we have successfully retrieved the differential SCDs of a gas over a series of measurements indexed t_i . If we assume the VCD as constant during the series of measurements, the differential SCD of a gas j at time t_i is:

$$\Delta s_j^{t_i} = \Delta \text{SCD}_j^{t_i} = \Delta \text{AMF}_j^{t_i} \cdot \text{VCD}_j \quad (1.10)$$

This is the equation of a line of slope VCD_j . Thus, by plotting the measured differential SCDs over the differential AMFs we expect to see a line, and the VCD is obtained by linear regression.

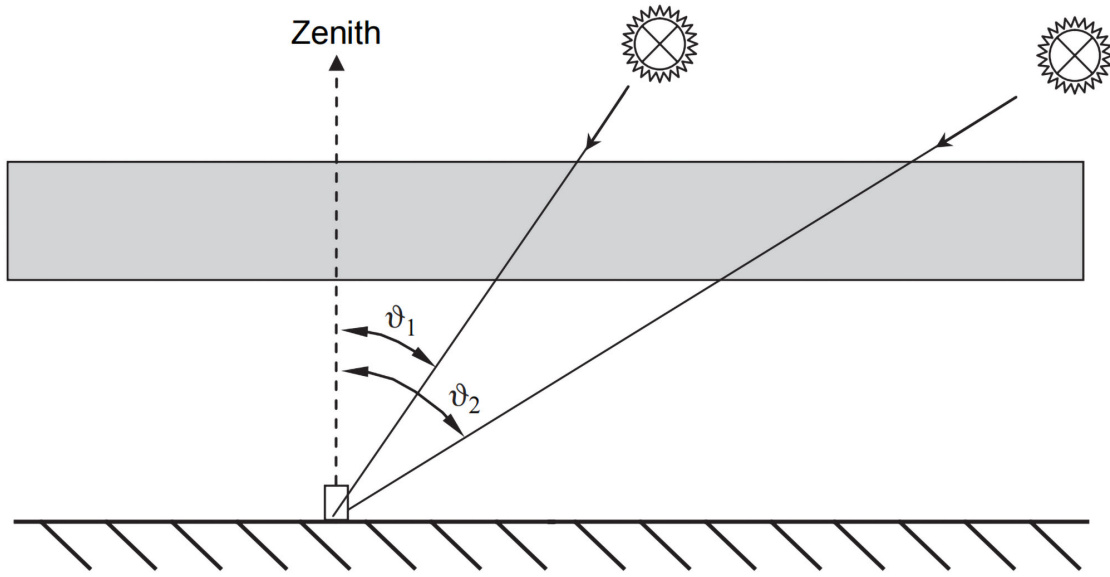


Figure 1: Sketch of direct light observation geometries. In first approximation, the light path through a trace gas layer varies with $1/\cos \theta$ (θ = solar zenith angle). From [1].

1.4 Focus on retrieving column densities of NO₂

Nitrogen dioxide (NO₂) primarily gets in the air from the burning of fuel [3]. It is a toxic and pollutant gas in the atmosphere that forms from emissions from cars, trucks and buses, power plants, and off-road equipment. Air with high NO₂ concentration can irritate airways in the human respiratory system. NO₂ along with other NO_x reacts with other chemicals in the air to form both particulate matter and ozone. Both of these are also harmful when inhaled due to effects on the respiratory system [3].

Its absorption range being approximately [300, 600 nm] (in wavelength) (Figure 2), it can be detected by our sensor, designed for UV-Vis spectrometry. We will limit our range of study to a small band centered on 400 nm, using an interferential filter. In this band, the absorption of NO₂ is dominant over the other gases of the atmosphere, and the absorption cross-section spectrum of NO₂ show quasi-periodic patterns (Figure 3), which is benefic as we measure interferograms that are linked to spectra through the Fourier transform, as we will see in section 2.3.

2 ImSPOC Acquisition Model

2.1 Sensor principle

The ImSPOC prototype is a CCD camera on which is mounted – from top to bottom – (a) a leading optical system, (b) a matrix of Fabry-Pérot interferometers, (c) the micro-lens matrix, and (d) the photodetector matrix which is on the focal plane [4].

Since we target the gas NO₂, we use an interferential filter on top of the optical system,

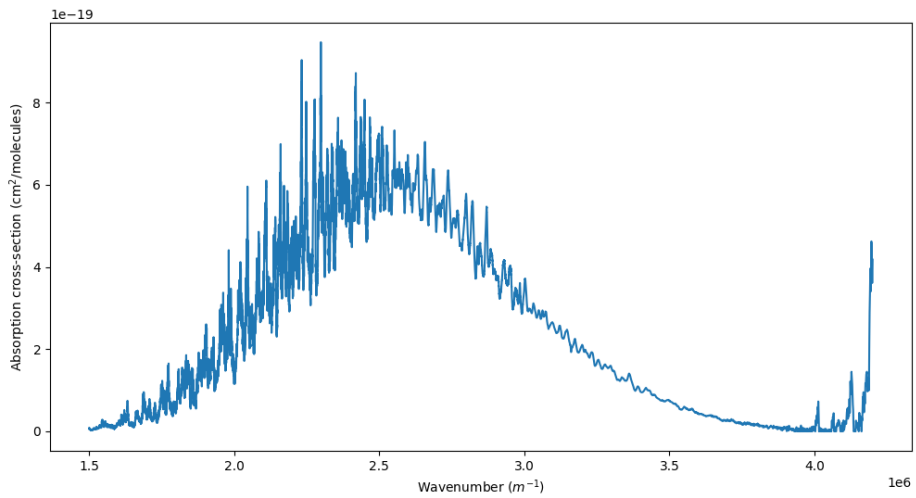


Figure 2: Absorption cross-section spectrum of NO_2 : $\alpha_{NO_2}(\sigma)$.

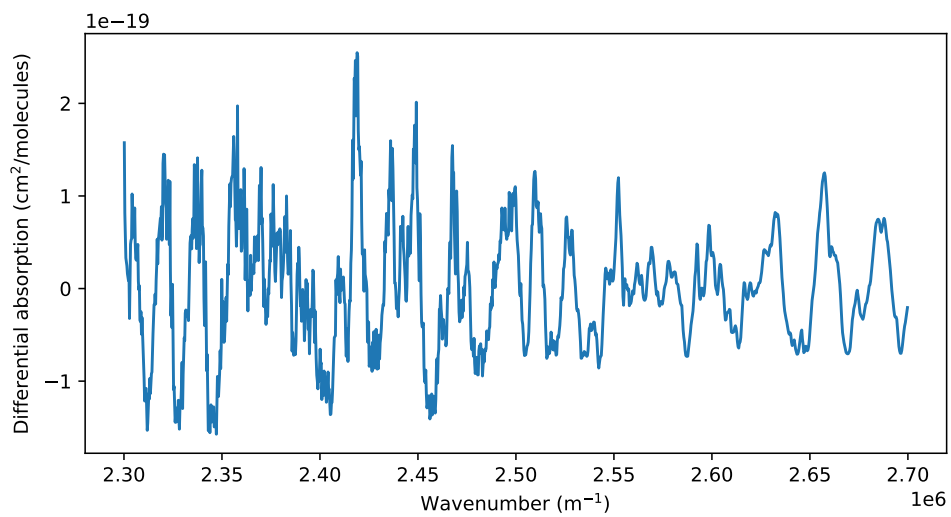


Figure 3: Differential absorption cross-section spectrum of NO_2 in the bandwidth of the interferential filter : $\widetilde{\alpha_{NO_2}}(\sigma)$.

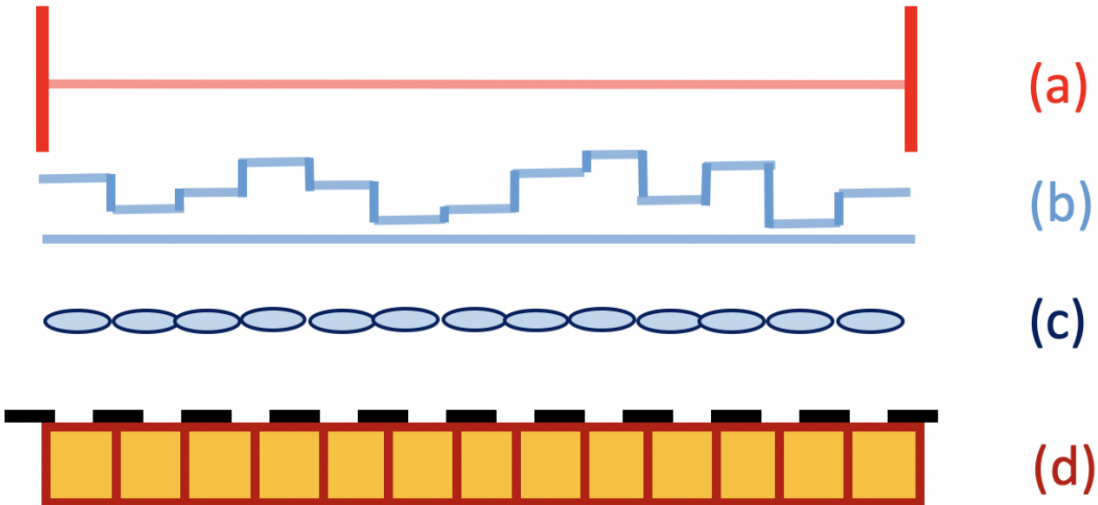


Figure 4: Scheme of the ImSPOC prototype with its components: (a) the leading optical system, (b) Fabry-Perot interferometer matrix, (c) the micro-lens matrix and (d) the photodetector matrix which is on the focal plane (in black dashes). From [4].

which acts on the incident spectrum as a bandpass filter of bandwidth [375 nm, 425 nm]. In this spectral band, our gas of interest has a dominant absorption over the other atmospheric gases. The spectral response $\mathcal{T}_f(\sigma)$ of the filter is given in figure 5.

2.2 Principles of Fabry-Pérot interferometry

A Fabry-Pérot cavity is an optical interferometer composed of two parallel reflecting surfaces represented in figure 7 [2]. Let us consider a wavefront of parallel waves of complex amplitude U_{in} entering the cavity from the top. The emerging waves U_k are such that the k -th wave is obtained by 2 transmissions across both surfaces and $2k$ reflections within the cavity. Their amplitude has the form

$$U_k = (1 - R)e^{-j\phi/2}R^{2k}e^{-j\phi}U_{in} \quad (2.1)$$

where R is the reflectivity of the cavity and ϕ the phase shift introduced by a round trip within the interferometer. If we consider the incoming wave quasi-monochromatic with a central wavenumber σ , then

$$\phi = 2\pi\sigma\delta \quad (2.2)$$

where δ is the **optical path difference (OPD)**. We can geometrically prove that

$$\delta = 2nL \cos \theta \quad (2.3)$$

The emerging waves interfere at infinity and form an emerging wavefront of energy intensity $I_{out} = \left| \sum_{k=1}^K U_k \right|^2$. We define the transmittance of the cavity as $\mathfrak{T} = I_{out}/I_{in}$.

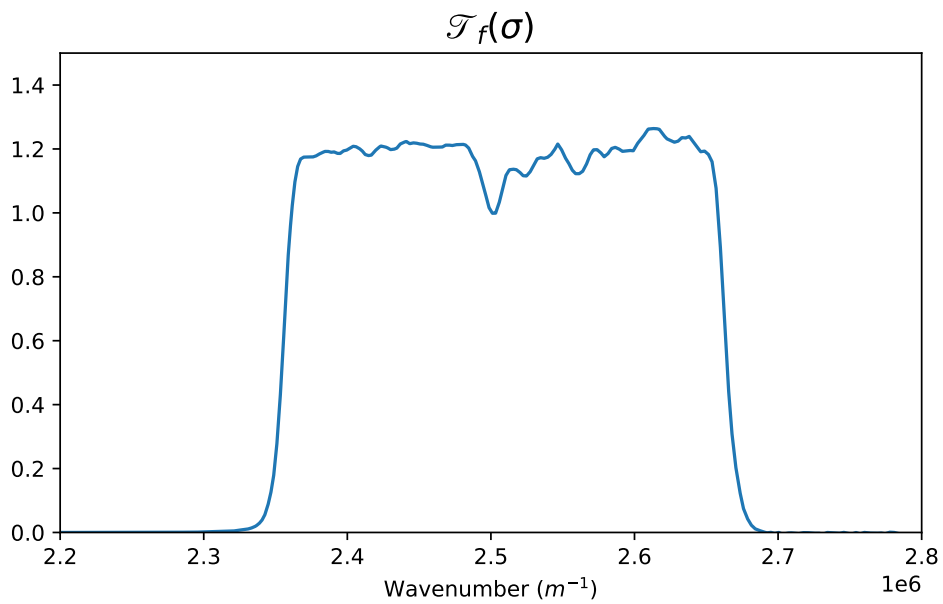
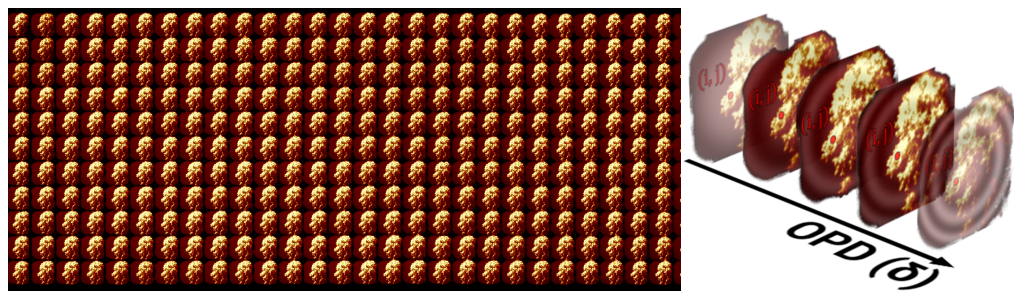


Figure 5: Transfer function of the interferential filter.



(a) Raw image acquired by *ImSPOC*

(b) Extracted thumbnails ordered by OPD. The interference fringes are amplified for understanding.

Figure 6: Raw data obtained with ImSPOC

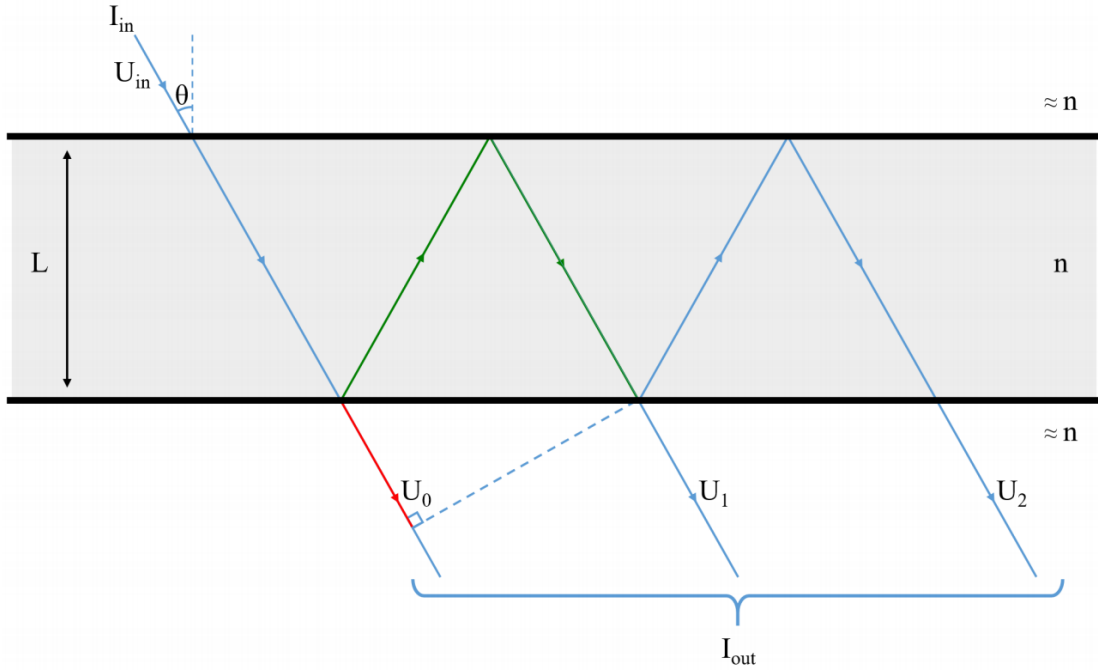


Figure 7: Scheme of a Fabry-Pérot cavity. From [2].

If we consider an infinite number of emerging waves, \mathfrak{T} can be expressed as:

$$\mathfrak{T}_{\infty} = \frac{(1-R)^2}{1-R^2} \left(1 + \frac{4R}{(1-R)^2} \sin\left(\frac{\phi}{2}\right) \right)^{-1} \quad (2.4)$$

If we only consider two emerging waves, its expression is:

$$\mathfrak{T}_2 = 1 + R^2 + 2R \cos(\phi) \quad (2.5)$$

Figure 8 shows the transmittance of a Fabry-Pérot cavity depending on its reflectivity. For low reflectivities, as for ImSPOC ($R=0.25$), the transmittance can be approximated by the two-wave model.

One can measure I_{out} by placing a convergent lens after the interferometer and a photodetector matrix on its focal plane so that the interferences are no longer located at infinity but on the focal plane. This is the configuration of the ImSPOC prototype (figure 4).

2.3 Modeling the sensor

Let $\mathcal{T}_{FP}(\sigma, \delta)$ be the transfer function of a Fabry-Pérot interferometer with OPD δ (which is linked to the thickness of a Fabry-Pérot cavity through (2.3)). The 2-wave model for its transmittance function is a good approximation:

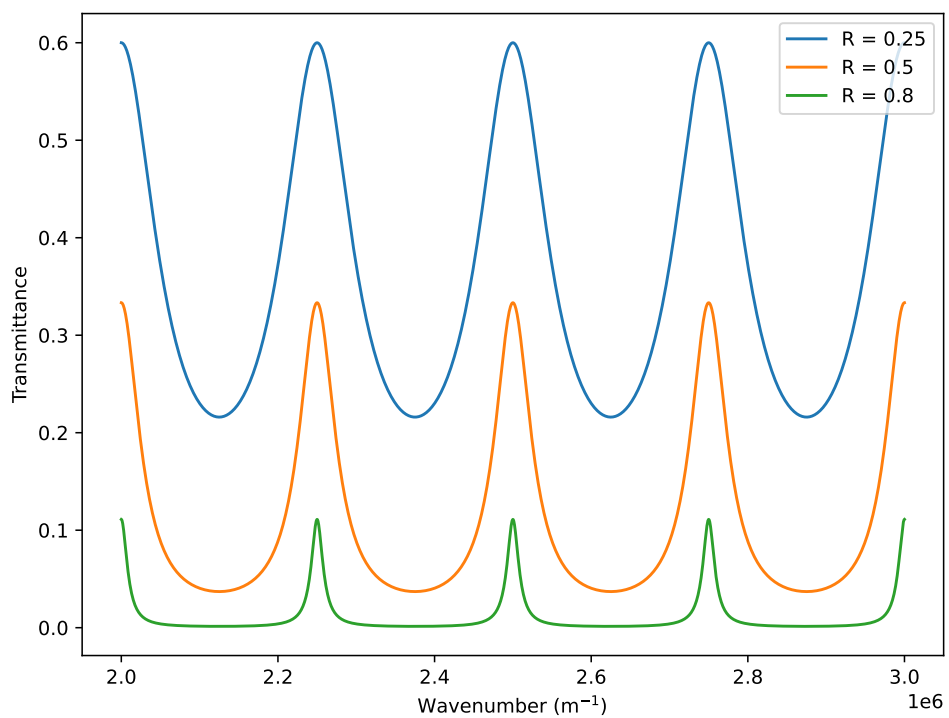


Figure 8: Filtering effect of a Fabry-Pérot cavity of thickness $\delta = 2\mu\text{m}$.

$$\mathcal{T}_{FP}(\sigma, \delta) = 1 + R^2 + 2R \cdot \cos(2\pi\sigma\delta) \quad (2.6)$$

Let $I_{out}^{ij}(\delta)$ be the intensity of a light ray that arrives on a photodetector corresponding to pixel (i, j) and OPD δ :

$$I_{out}^{ij}(\delta) = \int_0^{+\infty} \mathcal{T}_f(\sigma) \cdot \mathcal{T}_{FP}(\sigma, \delta) \cdot I_{in}^{ij}(\sigma) d\sigma \quad (2.7)$$

Notice that we do not take into account the transfer function of the instrument.

$$I_{out}^{ij}(\delta) = (1 + R^2) \int_0^{\infty} \mathcal{T}_f(\sigma) I_{in}^{ij}(\sigma) d\sigma + 2R \int_0^{\infty} \cos(2\pi\sigma\delta) \cdot \mathcal{T}_f(\sigma) I_{in}^{ij}(\sigma) d\sigma \quad (2.8)$$

$I_{out}^{ij}(\delta)$ is called an interferogram. Each interferometer has a different thickness L that yields a sample of this interferogram at the OPD $\delta \approx 2L$.

The second term of $I_{out}^{ij}(\delta)$ (its variable component) is equal, by a factor, to the real part of $I_{in}(\sigma)$'s Fourier transform. Thus a Fourier transform converts the interferogram into an actual spectrum and vice-versa.

$$I_{out}^{ij}(\delta) = \underbrace{(1 + R^2) \int_0^{\infty} \mathcal{T}_f(\sigma) I_{in}^{ij}(\sigma) d\sigma}_{\text{constant}} + R \cdot \underbrace{\text{Re}\{\mathcal{F}[I_{in}^{ij}(\sigma)](\delta)\}}_{\text{zero mean } (\delta > 0)} \quad (2.9)$$

We obtain $\text{Re}\{\mathcal{F}[I_{in}^{ij}(\sigma)](\delta)\}$ by subtracting to $I_{out}^{ij}(\delta)$ its mean value.

3 Python Module

Throughout the project, a Python module was developed to process the data acquired by ImSPOC, to transform them into interferograms, and to gather functions allowing to process the interferograms.

3.1 Raw data processing

The data to be processed is the snapshot focal plane intensity acquired by the detector. It is a mosaic of images, called *thumbnails*, of the observed scene seen through different interferometer thicknesses (see fig. 6a). The acquisitions are saved in FITS format (Flexible Image Transport System). A FITS file can contain several images and embed metadata in human-readable headers, such as timestamp, exposure time, etc. They are read using the Python module Astropy and processed inside a class *ImSPOCFits*. The images are stored in a list of *ImSPOCImages*.

An instance of *ImSPOCImage* contains extracted thumbnails, and the extracted interferograms (see next section 3.2).

A pixel s of an acquired image is expressed in analog-to-digital unit (ADU) and depends on the gain of the CCD sensor, which represents the conversion factor from electrons into digital counts.

$$s = d_{offset} + t_i \cdot G \int \eta(\sigma) L(\sigma) d\sigma$$

where t_i is the integration time (or exposure time), G is the gain of the CCD sensor, $\eta(\sigma)$ is the normalized instrumental spectral response function, and $L(\sigma)$ is the spectral radiance of the scene.

To convert the signal into a physical radiance, we subtract the dark image (an image taken with the sensor occulted) and divide by the integration time:

$$s' = \frac{s - d_{offset}}{t_i} = G \int \eta(\sigma) L(\sigma) d\sigma$$

Since we do not have radiometrically calibrated our instrument, we do not know G nor $L(\sigma)$. We neglect $L(\sigma)$ so that s' is equal to the total radiance I of the pixel with a constant factor.

3.2 Interferogram extraction

It is necessary to extract the thumbnails from a snapshot (figure 6a). For this the centers of the thumbnails are obtained through calibration [4], along with the interferometer thicknesses corresponding to each thumbnail. The OPD δ is linked to the interferometer thickness L through $\delta = 2L$ (this is an approximation, it would be ideal to know the value of the OPD corresponding to every pixel of a snapshot).

As each thumbnail is an image of the scene seen through an interferometer corresponding to OPD δ_k ($k \in \llbracket 1, 318 \rrbracket$), we obtain an interferogram $I^{ij}(\delta)$ by selecting the pixel (i,j) of every thumbnail ordered by OPD δ (figure 6b).

4 Measurements

We do our measurements with both the ImSPOC prototype and a reference spectrometer, so that we can apply the classical DOAS algorithm on the spectral data and obtain values of column densities we are confident about, to compare with ImSPOC. An ImSPOC capture is composed of a hundred snapshots taken at a rate of 5 snapshots per second, that are averaged into one image in order to maximize the signal-to-noise ratio (see section 6.1). The exposure time is adjusted so that the peak value in the image is in a range where the sensor is linear (and most importantly not saturated).

In zenithal observations, we orient our camera vertically towards the zenith (Figures 9a and 10a). In direct observations, our camera is oriented towards a Spectralon screen, which is a material with a high diffuse reflectance, that can be considered lambertian (angularly uniform). It is tilted to diffuse the sunlight so that the light received by the camera is mostly direct light (though there is a small part of scattered light).

In direct configuration, direct visibility of the sun is necessary and so the measurements are taken with a smaller AMF than in zenithal configuration for which we can begin and end the measurements when the solar zenith angle is very high (at sunrise and sunset).

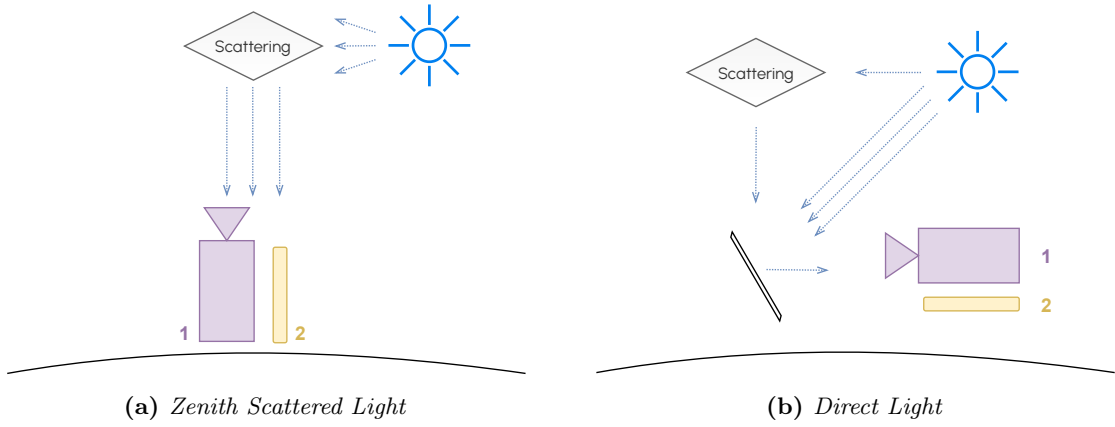


Figure 9: Acquisition scheme. 1 ImSPOC-UV2 camera, 2 OCEAN spectrometer. In zenith scattered light conditions (a), our instruments are directed to the zenith. In direct light conditions (b), our instruments are directed to a Spectralon diffuse reflectance material.

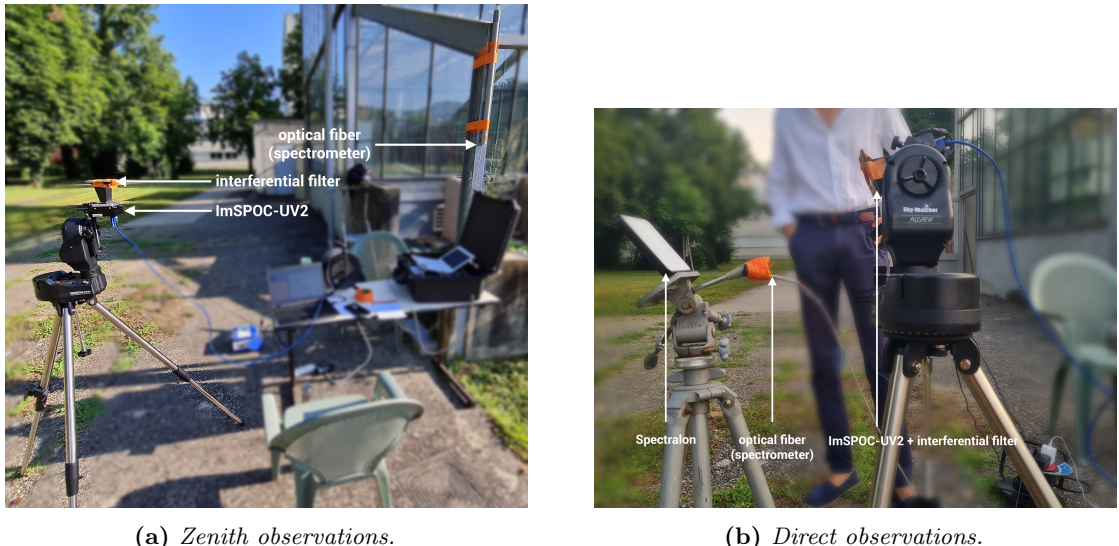


Figure 10: Capture setups for zenith and direct observations.

Nevertheless, considering only direct light makes the computation of the AMF easier and less dependant on the model. (see section 5.3)

The measurements are made under clear and sunny sky conditions.

5 Estimation of Column Densities

5.1 Beer-Lambert on interferograms

We showed that ImSPOC acquires interferograms, which are linked to spectra through the Fourier transform. Since the main goal of ImSPOC is to be a spectrometer, transfer matrix inversion techniques were already developed in order to retrieve a spectrum from an interferogram generated by the sensor. In this project, we explore the possibility of performing atmospheric gases measurements directly from interferograms instead of spectra obtained through inversion. As Beer-Lambert's law applies on spectra, we apply a Fourier transform to express the DOAS problem with the sensor data.

We recall the DOAS equation:

$$\ln \widetilde{\frac{I_{ref}(\sigma)}{I(\sigma)}} = \sum_j \Delta s_j \widetilde{\alpha_j}(\sigma) \quad (5.1)$$

$$I(\sigma) = \langle I \rangle(\sigma) + \widetilde{I}(\sigma) \quad (5.2)$$

where $\langle I \rangle(\sigma)$ is a low frequency component and $\widetilde{I}(\sigma)$ the variable component.

Assuming $\left| \frac{\widetilde{I}(\sigma)}{\langle I \rangle(\sigma)} \right| \ll 1$:

$$\begin{aligned} \ln \frac{I_{ref}}{I} &= \ln \frac{I_{ref}}{\langle I_{ref} \rangle} - \ln \frac{I}{\langle I \rangle} + \ln \frac{\langle I_{ref} \rangle}{\langle I \rangle} \\ &= \ln \left(1 + \frac{\widetilde{I}_{ref}}{\langle I_{ref} \rangle} \right) - \ln \left(1 + \frac{\widetilde{I}}{\langle I \rangle} \right) + \ln \frac{\langle I_{ref} \rangle}{\langle I \rangle} \\ &\approx \frac{\widetilde{I}_{ref}}{\langle I_{ref} \rangle} - \frac{\widetilde{I}}{\langle I \rangle} + \ln \frac{\langle I_{ref} \rangle}{\langle I \rangle} \end{aligned} \quad (5.3)$$

Then, since $\ln(\langle I_{ref} \rangle / \langle I \rangle)$ is low-frequency,

$$\ln \widetilde{\frac{I_{ref}(\sigma)}{I(\sigma)}} = \frac{\widetilde{I}_{ref}}{\langle I_{ref} \rangle} - \frac{\widetilde{I}}{\langle I \rangle} \stackrel{(5.1)}{=} \sum_j \Delta s_j \widetilde{\alpha_j}(\sigma) \quad (5.4)$$

We apply a Fourier transform on (5.4) and obtain:

$$\overline{I_{ref}}^{-1} \mathcal{F} \left[\widetilde{I_{ref}}(\sigma) \right] (\delta) - \overline{I}^{-1} \mathcal{F} \left[\widetilde{I}(\sigma) \right] (\delta) = \sum_j \Delta s_j \mathcal{F} [\widetilde{\alpha_j}(\sigma)] (\delta) \quad (5.5)$$

Where \overline{I} represents the mean value of $I(\sigma)$. However, even though we may estimate this value from the mean value of an interferogram (2.9), this equation did not yield any interesting result. Instead, we introduce a scaling factor c_1 to account for experimental discrepancies and to better model our later results:

$$\mathcal{F} \left[\widetilde{I}_{ref}(\sigma) \right] (\delta) - \mathcal{F} \left[\widetilde{I}(\sigma) \right] (\delta) = c_1 \sum_j \Delta s_j \mathcal{F} [\widetilde{\alpha}_j(\sigma)] (\delta) \quad (5.6)$$

Going back to our expression of a measured interferogram $I_{out}^{ij}(\delta)$, we can rewrite (2.9) as:

$$\text{Re}\{\mathcal{F}[I_{in}^{ij}(\sigma)](\delta)\} = I_{out}^{ij}(\delta) - \overline{I_{out}^{ij}(\delta)} \quad (5.7)$$

where $\overline{I_{out}^{ij}(\delta)}$ is the mean value of the interferogram. Since our sensor prototype is not perfect and the illumination of an interferometer can vary, we subtract to the interferogram a fitted polynomial of low degree (typically ≈ 5).

Finally,

$$\begin{aligned} \widetilde{\Delta I}(\delta) &\stackrel{\text{def}}{=} \left(I_{ref}^{ij}(\delta) - \overline{I_{ref}^{ij}(\delta)} \right) - \left(I^{ij}(\delta) - \overline{I^{ij}(\delta)} \right) \\ &= c_1 \sum_j \Delta s_j \mathcal{F} [\widetilde{\alpha}_j(\sigma)] (\delta) \end{aligned} \quad (5.8)$$

From this equation, one could perform a curve-fitting method in a similar fashion as for the DOAS on spectra. However, our attempts with this method were unsuccessful. In reality, the $\widetilde{\Delta I}$ we get are not only composed of the sum in (5.8), as there seems to be an additive signal which we model as $N(\delta)$:

$$\widetilde{\Delta I}(\delta) = N(\delta) + c_1 \sum_j \Delta s_j \mathcal{F} [\widetilde{\alpha}_j(\sigma)] (\delta) \quad (5.9)$$

5.2 Gas correlation

Another idea to retrieve Δs_{NO_2} is to correlate $\widetilde{\Delta I}(\delta)$ with $\mathcal{F} [\widetilde{\alpha}_{\text{NO}_2}] (\delta)$, i.e. compute their covariance:

$$\text{Cov} \left(\widetilde{\Delta I}(\delta), \mathcal{F} [\widetilde{\alpha}_{\text{NO}_2}] (\delta) \right) = \int \widetilde{\Delta I}(\delta) \mathcal{F} [\widetilde{\alpha}_{\text{NO}_2}] (\delta) d\delta \quad (5.10)$$

(note that $\widetilde{\Delta I}$ and $\mathcal{F} [\widetilde{\alpha}_{\text{NO}_2}]$ have zero mean)

We suppose:

- $\text{Cov}(N, \mathcal{F} [\widetilde{\alpha}_{\text{NO}_2}]) \approx 0$ i.e. the noise and $\mathcal{F} [\widetilde{\alpha}_{\text{NO}_2}]$ are not correlated
- $\forall j \neq \text{NO}_2, \text{Cov}(\mathcal{F} [\widetilde{\alpha}_j], \mathcal{F} [\widetilde{\alpha}_{\text{NO}_2}]) \approx 0$ i.e. NO_2 's absorption cross-section is not correlated to that of other considered gases

Then, because the covariance is bilinear:

$$\begin{aligned}\text{Cov} \left(\widetilde{\Delta I(\delta)}, \mathcal{F} [\widetilde{\alpha_{\text{NO}_2}}] (\delta) \right) &= \text{Cov} \left(c_1 \Delta s_{\text{NO}_2} \mathcal{F} [\widetilde{\alpha_{\text{NO}_2}}], \mathcal{F} [\widetilde{\alpha_{\text{NO}_2}}] \right) \\ &= \Delta s_{\text{NO}_2} \cdot \underbrace{c_1 \text{Var} (\mathcal{F} [\widetilde{\alpha_{\text{NO}_2}}])}_{c_2}\end{aligned}\quad (5.11)$$

Thus, the covariance between $\widetilde{\Delta I}$ and $\mathcal{F} [\widetilde{\alpha_{\text{NO}_2}}]$ is proportional to the (difference of) SCD of NO_2 . Since we do not have a radiometric calibration of our instrument, as explained in section 3.1, our measurement of $\widetilde{\Delta I}$ has a certain gain G , so the computed covariance is equal to $\Delta s_{\text{NO}_2} \cdot c_3$ with $c_3 = G \cdot c_2$. We get rid of this constant by calibration, having a measured covariance and a reference value of the expected differential SCD.

5.3 AMF calculation

In order to finally get a vertical column density (VCD) from the slant column density (SCD), the air-mass factor (AMF) must be determined. Because the covariance in (5.11) is proportional to the SCD, it is proportional to the VCD and AMF (1.9). Thus, plotting the SCD as a function of the AMF should result in a line of slope equal to the VCD.

The determination of the AMF requires to take into account different physical processes influencing the radiative transfer in the atmosphere, such as scattering processes, reflection on the earth's surface, the curvature of the earth, refraction, and the distribution of trace gases [1]. Thereby, it relies on the development a radiative transfer model, which is a complex task.

For scattered zenith light measurements, a simple radiative transfer model was implemented, based on Sarkissian's model, using the data presented in the thesis [5]. This model simulates the paths of 60 parallel light rays scattered at every altitude of the atmosphere decomposed in homogeneous layers of 1 km thickness, from 0 to 60 km. We only consider rays of wavelength 400 nm, since it is the center wavelength of the interferential filter in use with the sensor. The obtained AMF is shown in Figure 11. However, our modeling seems incorrect at high solar zenith angle ($> 88^\circ$), when the AMF is maximal and the measurement of the SCD is the most sensitive to NO_2 .

For direct light measurements, we can approximate the AMF with the geometrical AMF which only depends on the solar zenith angle ($\text{AMF} = 1 / \cos \theta$), but again this approximation is incorrect for high angles.

6 Results

6.1 Simulation and noise considerations

Our reference values of NO_2 column density are taken from publicly available ground-based SAOZ data in Observatoire de Haute-Provence (OHP), which is a UV-visible spectrometer designed for measurements of atmospheric profiles of minor chemical species (O_3 , H_2O , NO_2 , O_2 , O_4 , BrO , OCIO , CH_2O) by zenithal observation. At the time of the internship, in summer 2021, the vertical column density of NO_2 in OHP is around

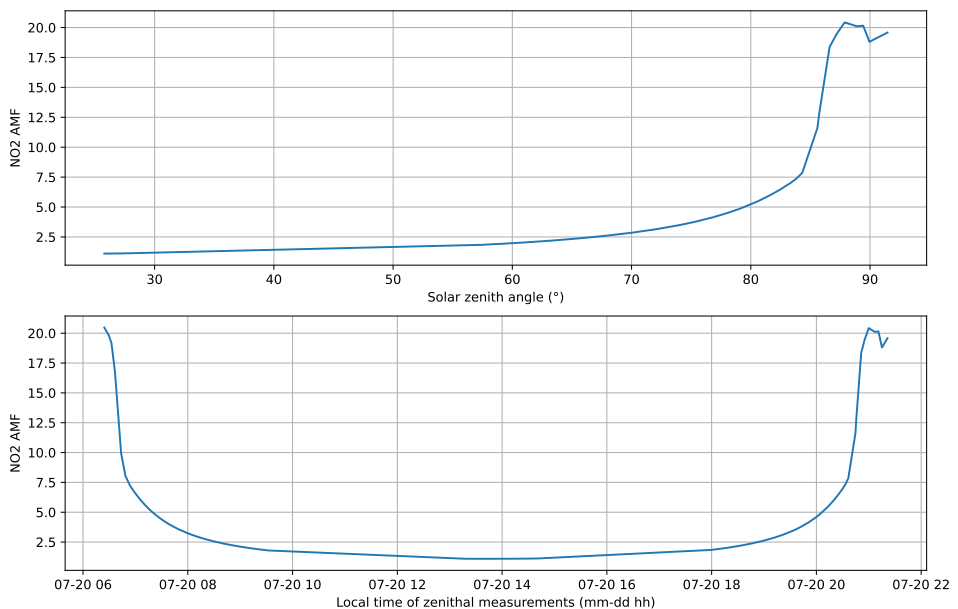


Figure 11: Calculated AMF of zenith scattered light with Sarkissian's model, shown in function of the solar zenith angle and in function of time.

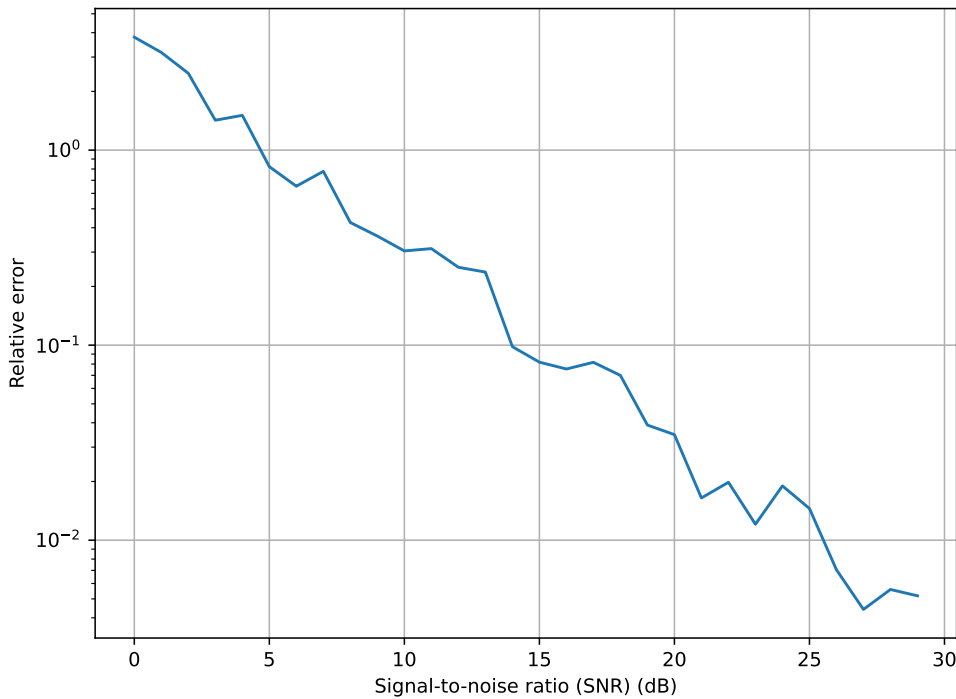


Figure 12: Relative error on the estimated vertical column density (with an exact value of $3 \cdot 10^{15}$ molecules/cm²) on simulated interferograms in function of the signal-to-noise ratio (SNR). The relative error drops under 1% for a minimum SNR of 26 dB.

$3 \cdot 10^{15}$ molecules/cm² at sunrise, and $5 \cdot 10^{15}$ molecules/cm² at sunset. Therefore the maximum optical density of NO₂ measurable, when the AMF is maximum (two to three tens), has the order of magnitude 0.01 (-20 dB).

We have simulated the expected interferograms by modeling spectra with Beer-Lambert's law, considering only the extraterrestrial solar spectrum and the absorption cross-section of NO₂ (ideal case without other extinction events, such as other trace gases). Figure 12 shows the relative error on the estimated vertical column density, using the correlation method (section 5.2), with our simulated interferograms. We vary the signal-to-noise ratio (SNR) by adding a gaussian noise on the spectra before we transform them into interferograms, sampled at ImSPOC's OPDs. For each value of SNR, the spectra are generated with a VCD of $3 \cdot 10^{15}$ and an AMF varying between 10 and 20 (11 spectra). We repeat this process 10 times to obtain an average value of the relative error.

6.2 Results

We applied the gas correlation method shown in section 5.2 to our measurements: we use an interferogram taken when the sun is at its zenith as a reference. For every interferograms we compute their difference with the reference and correlate it with NO₂.

Zenith scattered light measurements

Figures 13 and 14 show NO₂ correlation (or covariance) with differential interferograms in function of time. Its evolution should be compared to the evolution of the AMF in Figure 11. Negative or close-to-zero values mean there is no correlation. This is the case of the points taken at noon, which are also very noisy. This is expected since we measure differential columns using an interferogram at noon as a reference, thus the differential column is too small compared to the noise level.

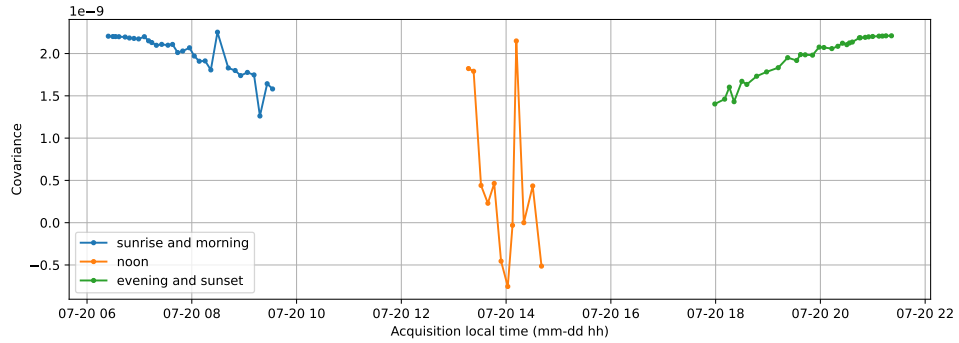


Figure 13: NO₂ correlation (or covariance) in function of time for zenith scattered light measurements.

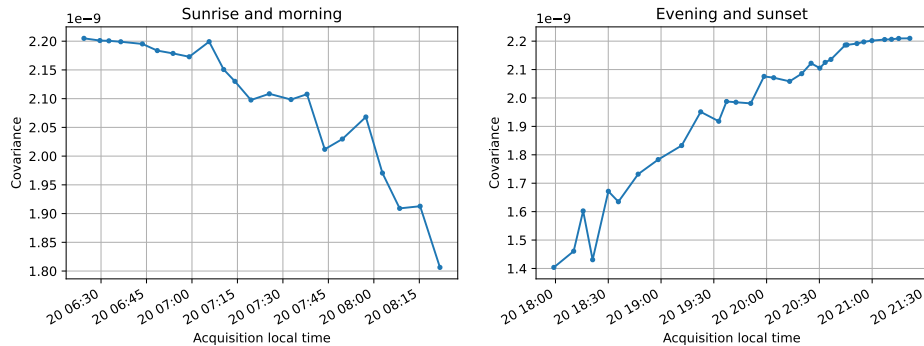


Figure 14: NO₂ correlation (or covariance) in function of time for zenith scattered light measurements at morning and at evening.

In Figure 15 we plot the covariance no longer in function of time but of the AMF. While we expect to see a line of slope proportional to the desired VCD, the result is not

a line on the whole extent of AMF. In order to go further, a more precise calculation (or measurement) of the AMF is necessary.

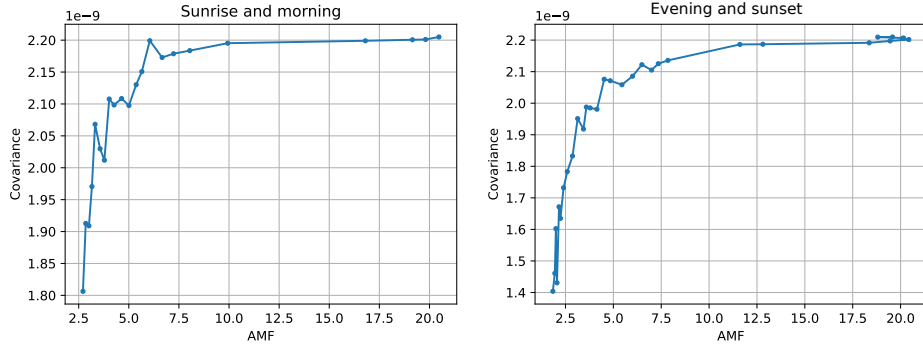


Figure 15: NO_2 correlation (or covariance) in function of the calculated AMF (fig. 11) for zenith scattered light. We fail to obtain a line on a satisfying extent of AMF, probably because the calculated AMF is incorrect.

Direct light measurements

In direct light configuration, we could not manage to have good visibility at sunrise nor sunset from our location, so we only have data for low-AMF light, when the sun was elevated enough. Plotting the covariance in function of the geometrical AMF (Figure 16) yields a line only on a small extent of AMF:

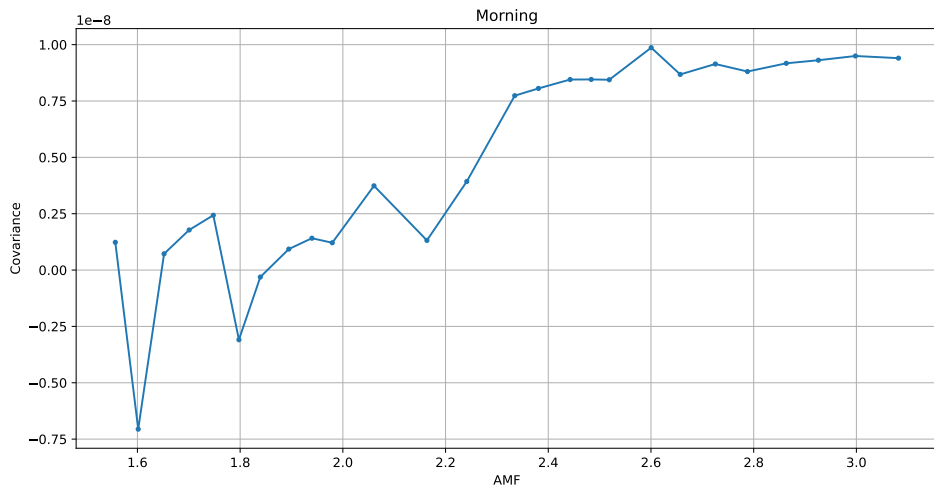


Figure 16: NO_2 correlation (or covariance) in function of the geometrical AMF (fig. 11) for direct light. The correlation is bad for points with AMF under 2.3.

Conclusion

In this work, we have explored the possibility of retrieving vertical column densities of gases, NO₂ in particular, with a Fourier transform imaging spectrometer based on an array of Fabry-Pérot interferometers, which is still at the prototype stage. More specifically, we proposed a method adapted from the existing DOAS technique which applies not on spectra but interferograms, while current developments focus on the inversion of interferograms. The obtained results, through simulation and measurements, show potential and give us better insight into the device. However, more developments on the determination of air mass factors are necessary to go further and validate the results.

References

- [1] Platt, U., & Stutz, J. (2008). Differential absorption spectroscopy. In *Differential Optical Absorption Spectroscopy* (pp. 135-174). Springer, Berlin, Heidelberg.
- [2] Picone, D., Dolet, A., Gousset, S., Voisin, D., Dalla Mura, M., & Le Coarer, E. (2020, May). Characterisation of a Snapshot Fourier Transform Imaging Spectrometer Based on an Array of Fabry-Perot Interferometers. In *ICASSP 2020-2020 IEEE International Conference on Acoustics, Speech and Signal Processing (ICASSP)* (pp. 1529-1533). IEEE.
- [3] EPA – United States Environmental Protection Agency. <https://www.epa.gov/no2-pollution/basic-information-about-no2> (visited in August 2021)
- [4] Dolet, A., Picone, D., Dalla Mura, M., Voisin, D., Gousset, S., Douté, S., & Le Coarer, E. (2019, October). Gas characterisation based on a snapshot interferometric imaging spectrometer. In *Image and Signal Processing for Remote Sensing XXV* (Vol. 11155, p. 1115502). International Society for Optics and Photonics.
- [5] Alain Sarkissian. Observation depuis le sol des nuages et des poussières dans l'atmosphère. Applications à la stratosphère polaire et à l'atmosphère de Mars. Physique Atmosphérique et Océanique [physics.ao-ph]. Université Pierre et Marie Curie - Paris VI, 1992. Français. ⟨NNT : 1992PA066326⟩. ⟨tel-00747520⟩
- [6] Gousset, S., Rodrigo, J. M., Le Coarer, E., Ehrhardt, H., Stadler, E., Hubert, Z., ... & Gerges, N. (2021, June). NanoCarb spaceborne miniaturized GHG sensor: first experimental results. In *International Conference on Space Optics—ICSO 2020* (Vol. 11852, p. 118522L). International Society for Optics and Photonics.
- [7] Gousset, S., Croize, L., Le Coarer, E., Ferrec, Y., Rodrigo-Rodrigo, J., & Brooker, L. (2019). NanoCarb hyperspectral sensor: on performance optimization and analysis for greenhouse gas monitoring from a constellation of small satellites. *CEAS Space Journal*, 11(4), 507-524.

- [8] Kuhn, J., Platt, U., Bobrowski, N., & Wagner, T. (2019). Towards imaging of atmospheric trace gases using Fabry–Pérot interferometer correlation spectroscopy in the UV and visible spectral range. *Atmospheric Measurement Techniques*, 12(1), 735–747.



Phelma



Appendix: Jupyter Notebook for the processing of zenith scattered light measurements

```
In [30]: %%html
<style type='text/css'>
.CodeMirror{
  font-size: 8px;
}</style>
```

```
In [1]: %matplotlib inline
from ImSPOC import ImSPOCFits, ImSPOCImage
import ImSPOC
import numpy as np
import os
from renaults.renaults import show, subplot
from scipy.io import loadmat
from os.path import join as _j
import scipy.interpolate
import matplotlib.pyplot as plt
import scipy.signal
import glob
import datetime
from datetime import timezone

plt.rcParams['figure.figsize'] = [12, 4] # 26 4
plt.rcParams['figure.dpi'] = 70
plt.close('all')

# on charge les centres des vignettes et les OPD, obtenus par calibration préalable
centers = loadmat('../support/pos_cen_N02.mat')['pos_cen']
OPD = loadmat('../support/deltaImSPOCUV2N02.mat')['delta'].reshape(-1)
OPD = 1e-6 * OPD # en μm
OPD_sorted = np.sort(OPD)

## pour choisir le dossier racine
ROOT = '/run/media/yann/Data/'
#ROOT = 'F:/'
```

chargement des données

```
In [2]: acqs, darks = ImSPOC.load_july_20_dataset(_j(ROOT, 'ige_imspoc_20-23-juil', 'IGE-20-07'), centers, OPD, verbose=False)
```

```
In [3]: _ = np.load('../support/SOLAR_ISS_V1.npz')
_wvn, _spectrum = _['wvn']*100, _['spectrum']
spectrum_interp = scipy.interpolate.interp1d(_wvn, _spectrum, fill_value=0, bounds_error=False)

N02 = ImSPOC.load_hitran('../support/N02_220.0_0.0_15002.0-42002.3_00.xsc')

wvn = np.linspace(N02['wvn_start'], N02['wvn_end'], num=len(N02['data']))
xs_interp = scipy.interpolate.interp1d(wvn, N02['data'], fill_value=0, bounds_error=False)

_= np.load('../support/filtre_reponse.npz')
_sig, _H = 1e9/_['lamb'][::-1], _['H'][::-1]
H_interp = scipy.interpolate.interp1d(_sig, _H, fill_value=0, bounds_error=False)

wvn2 = np.arange(0, 2.75e6, np.mean(np.diff(wvn)))
```

on calcule les transformées de Fourier de façon naïve afin de les évaluer aux OPD (~ fréquences) correspondant à ImSPOC, il n'y aura que 318 points

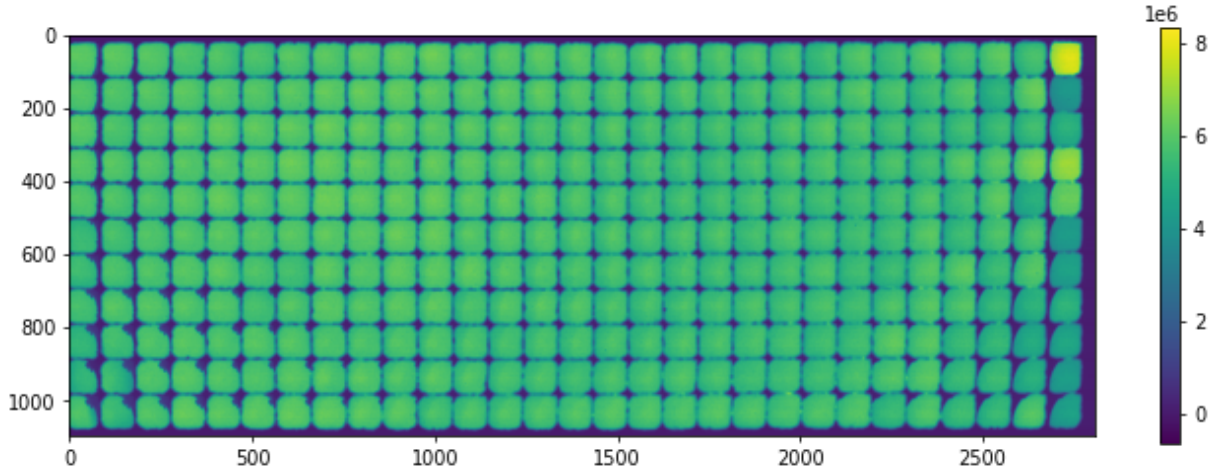
```
In [4]: def fourier(signal, time, freq):
    signal, freq = np.array(signal), np.array(freq)
    S = np.zeros(freq.size)
    for i, f in enumerate(freq):
        S[i] = np.sum(signal*np.cos(2*np.pi*f*time))
    return S
```

on précalcule la transformée de la section efficace d'absorption du NO₂ multipliée par le filtre interférentiel

```
In [5]: F_xs = fourier(xs_interp(wvn2)*H_interp(wvn2), wvn2, OPD_sorted)
```

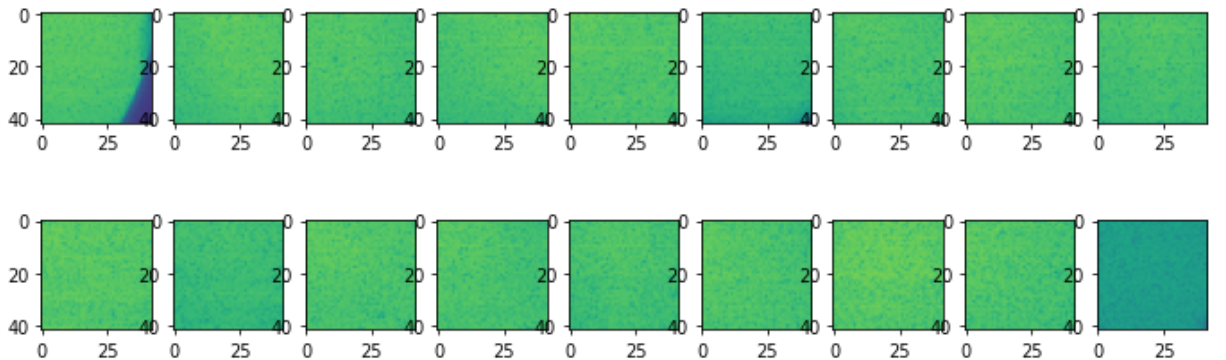
Image brute acquise

```
In [6]: show(acqs.images[-1].data, colorbar=True)
```



Quelques vignettes extraites

```
In [7]: show(*[acqs.images[-1].thumbs[i] for i in range(0,300,17)], nrows=2, vmin=np.min(acqs.images[-1].data), vmax=np.max(acqs.images[-1].data))
```

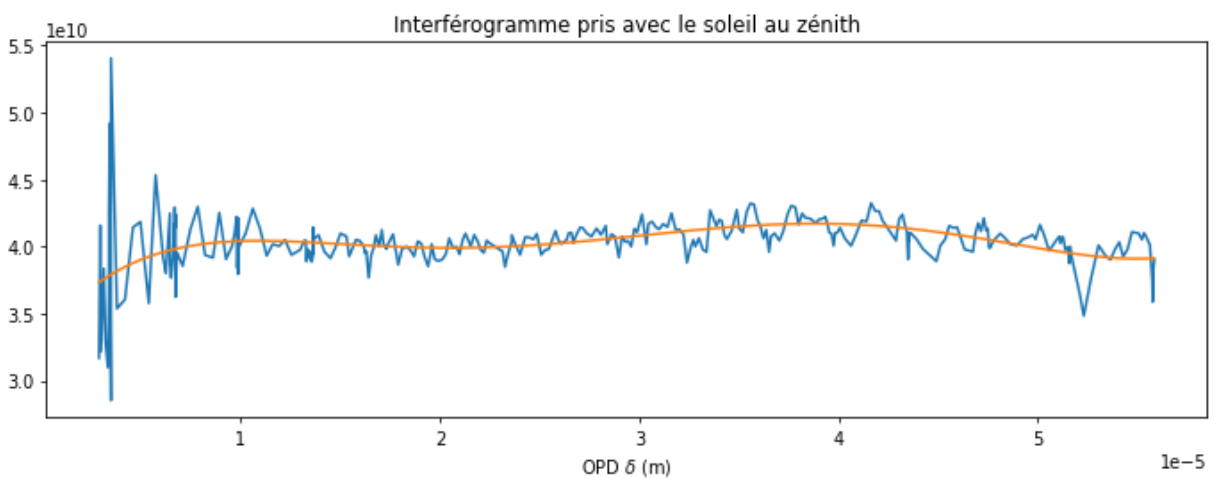


```
In [8]: center = (8,8)
avg = 5
```

on moyenne les pixels dans un carré de côté 5 centré en (8,8)

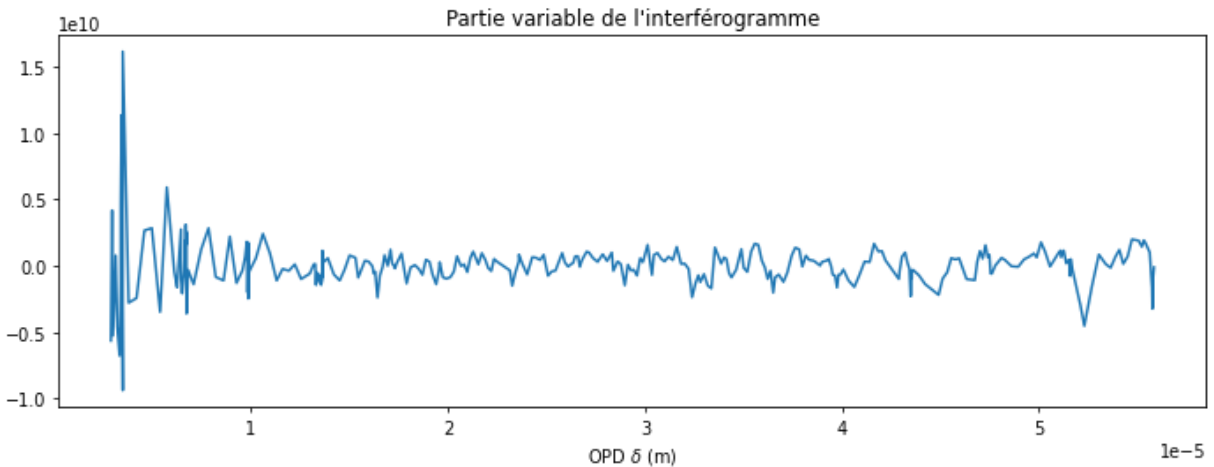
```
In [9]: _interf0 = acqs.images[40].average(*center, avg)
```

```
In [10]: plt.plot(OPD_sorted, _interf0)
_interf0_cut = ImSPOC.low_cut_poly(OPD_sorted, _interf0, 5)
plt.plot(OPD_sorted, _interf0 - _interf0_cut)
plt.title('Interférogramme pris avec le soleil au zénith')
plt.xlabel('OPD $\delta$ (m)');
```



On soustrait la valeur moyenne à l'interférogramme afin de n'avoir que sa partie variable. Pour prendre en compte les défauts d'illumination variable des vignettes, on approxime l'interférogramme par un polynôme de degré 5, et on y soustrait ce polynôme.

```
In [11]: plt.plot(OPD_sorted, _interf0_cut);
plt.title("Partie variable de l'interférogramme")
plt.xlabel('OPD $\delta$ (m)');
```



même chose pour un interférogramme acquis à une autre heure (au lever du soleil)

```
In [12]: _interf1 = acqs.images[0].average(*center, avg)
```

```
In [13]: interf0 = ImSPOC.low_cut_poly(OPD_sorted, _interf0, 5)
interf1 = ImSPOC.low_cut_poly(OPD_sorted, _interf1, 5)
```

$$\mathcal{F}^*[x] \triangleq \mathcal{F}[x \cdot \mathcal{T}_{filtre}]$$

On calcule la différence entre l'interférogramme de référence et l'interférogramme au lever du soleil.

$$\Delta I(\delta) = I_0(\delta) - I_1(\delta) = \sum_j \mathcal{F}^*[\mathrm{XS}_j(\sigma)](\delta) \cdot \Delta s_j$$

Pour retrouver Δs_{NO2} , on calcule la covariance entre $\Delta I(\delta)$ et $\mathcal{F}^*[\mathrm{XS}_j(\sigma)](\delta)$. Cette covariance est proportionnelle à Δs_{NO2} .

elle se calcule ainsi :

$$Cov (\mathcal{F}^*[\mathrm{XS}_{NO2}(\sigma)] ; \Delta I(\delta)) = \int \mathcal{F}^*[\mathrm{XS}_{NO2}(\sigma)] \cdot \Delta I(\delta) \, d\sigma$$

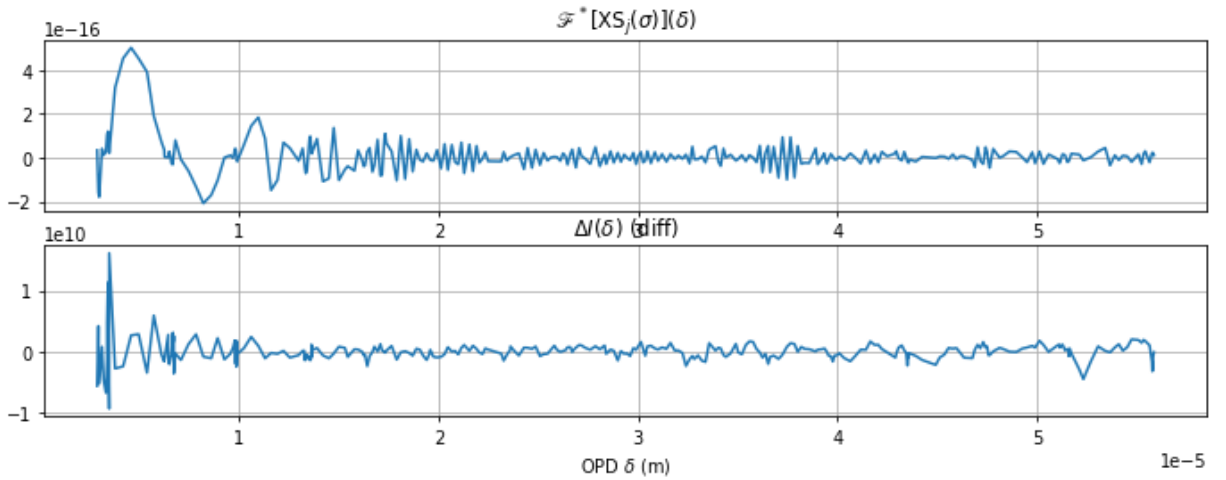
hypothèse : $\forall j \neq NO_2, Cov (\mathcal{F}^*[\mathrm{XS}_j(\sigma)] \cdot \Delta s_j ; \mathcal{F}^*[\mathrm{XS}_{NO2}(\sigma)]) \approx 0$

$$Cov (\mathcal{F}^*[\mathrm{XS}_{NO2}(\sigma)] ; \Delta I(\delta)) = a \cdot \Delta s_{NO2}$$

où a est une constante

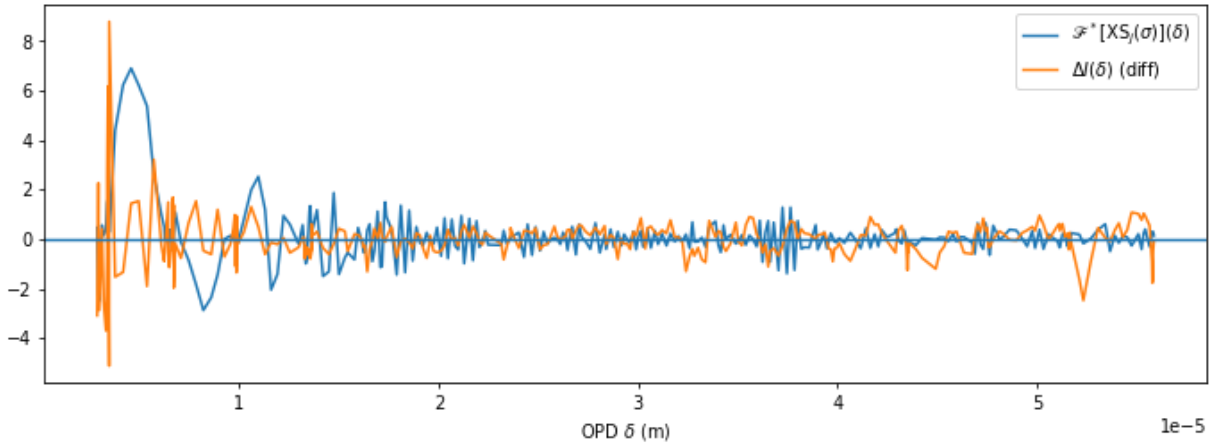
```
In [14]: diff = interf0 - interf1
```

```
In [15]: plt.subplot(2,1,1)
plt.title('$\mathcal{F}^*[\mathrm{XS}_j(\sigma)](\delta)$')
plt.plot(OPD_sorted, F_xs)
plt.xlabel('OPD $\delta$ (m)')
plt.grid()
plt.subplot(2,1,2)
plt.title('$\Delta I(\delta)$ (diff)')
plt.plot(OPD_sorted, diff)
plt.grid()
plt.xlabel('OPD $\delta$ (m)');
```

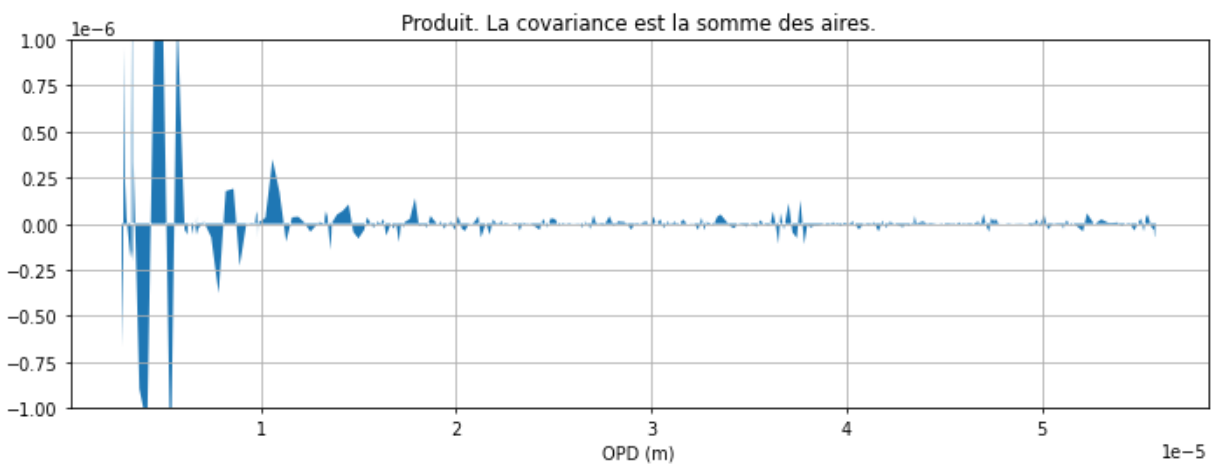


remarque : les signaux sont échantillonnés aux OPD d'ImSPOC (318 points, non-uniforme)

```
In [16]: plt.plot(OPD_sorted, F_xs/np.std(F_xs), label="$\mathcal{F}^*[XS_j(\sigma)](\delta)$")
plt.plot(OPD_sorted, diff/np.std(diff), label="$\Delta I(\delta) (diff)$")
plt.axhline(0)
plt.legend()
plt.xlabel('OPD $\delta$ (m)');
```



```
In [17]: plt.title('Produit. La covariance est la somme des aires.')
plt.fill_between(OPD_sorted, F_xs*diff)
plt.grid()
plt.ylim((-1e-6, 1e-6))
plt.xlabel('OPD (m)');
```



Nous calculons la covariance en ne sommant qu'à partir de l'OPD 10 μm (1e-5 m) afin de ne pas prendre en compte les faibles OPD.

```
In [18]: def utc_to_local(utc_dt):
    return utc_dt.replace(tzinfo=timezone.utc).astimezone(tz=None)
```

Nous répétons ce processus pour chaque acquisition :

In [19]:

```
times = []
corrs = []

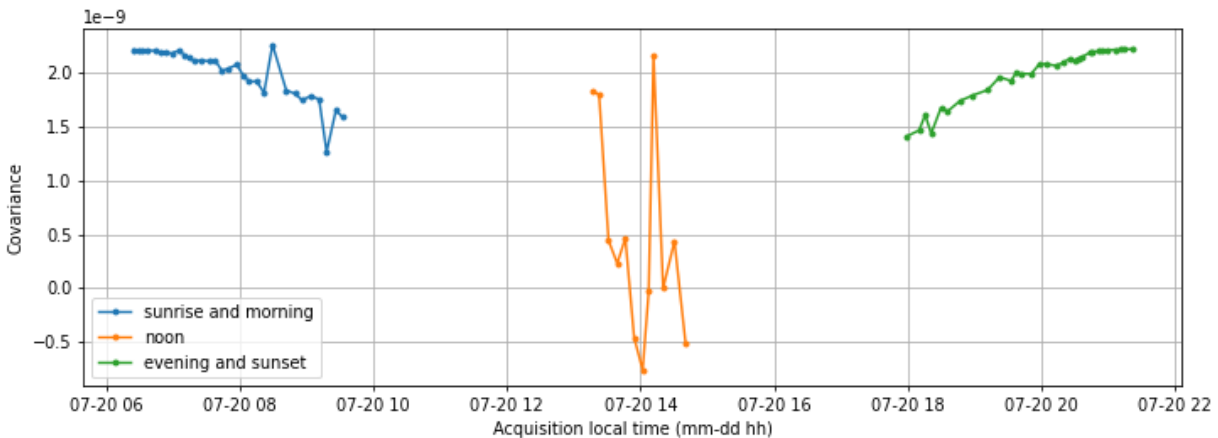
for i in range(len(acqs.images)):
    _interf = acqs.images[i].average(*center, avg)
    interf = ImSPOC.low_cut_poly(OPD_sorted, _interf, 5)
    diff = interf0 - interf

    mask = (OPD_sorted>10e-6) * (OPD_sorted<40e-6)
    corr = np.sum(mask*diff*F_xs)/np.sum(mask)

    times.append(acqs.images[i].datetime)
    corrs.append(corr)

localtimes = [utc_to_local(t) for t in times]

plt.figure(figsize=(12,4))
plt.plot(localtimes[:31], corrs[:31], label='sunrise and morning', marker='.')
plt.plot(localtimes[31:43], corrs[31:43], label='noon', marker='.')
plt.plot(localtimes[43:], corrs[43:], label='evening and sunset', marker='.')
plt.xlabel('Acquisition local time (mm-dd hh)')
plt.ylabel('Covariance')
plt.grid()
plt.legend();
# plt.savefig('../report/img/res-zenith-cov.pdf')
```



Retrouver la colonne verticale de NO₂

nous avons maintenant besoin du facteur de masse d'air (AMF) pour retrouver la colonne verticale de NO₂ :

$$\text{SCD} = \text{AMF} \cdot \text{VCD}$$

$$\text{or } \text{Cov} (\mathcal{F}^*[\text{XS}_{\text{NO}_2}(\sigma)] ; \Delta I(\delta)) = a \cdot \Delta \text{SCD}_{\text{NO}_2} = a \cdot \Delta \text{AMF}_{\text{NO}_2} \cdot \text{VCD}_{\text{NO}_2}$$

Pour des angles solaires zénithaux suffisamment faibles on utilise l'AMF calculé avec un modèle de transfert radiatif simple, mais pour des angles plus élevés (comme au coucher) nous utilisons une formule pour un AMF en lumière directe :

$$\text{AMF} = [\cos(Z) + .15 \cdot (93.885 - Z)^{-1.253}]^{-1} \text{ où } Z \text{ est l'angle solaire zénithal}$$

(formule tirée de https://www2.jpl.nasa.gov/adv_tech/photovol/2016CTR/SERI%20-%20Solar%20Spec%20for%20Dir%20&%20Dif%20Irrad%20on%20Planes_1984%20.pdf)

In [20]:

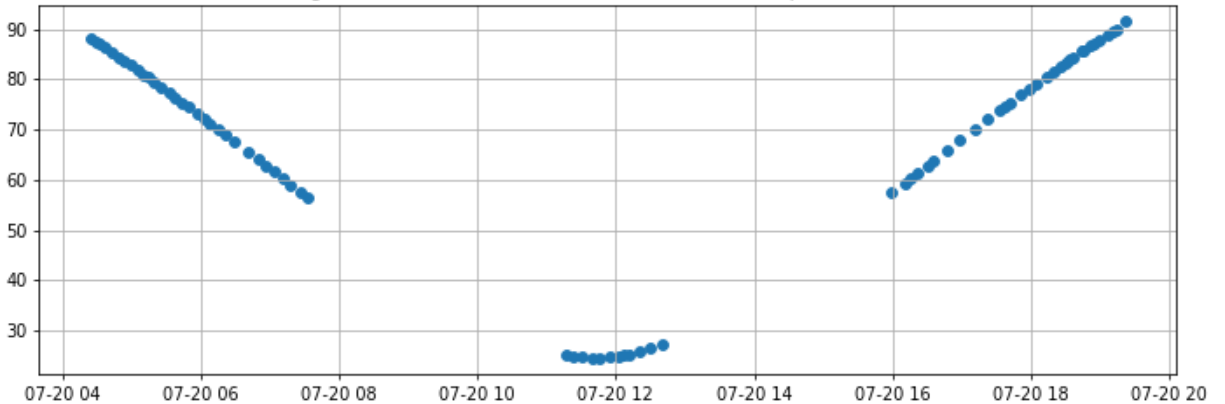
```
from datetime import timezone
import pysolar
Z = []
for time in times:
    dt = time.replace(tzinfo=timezone.utc)
    lat, lon = 45.19, 5.762
    alt = pysolar.solar.get_altitude(lat, lon, dt)
    SZA = 90 - alt
    Z.append(SZA)
Z = np.array(Z)
```

```
/home/yann/anaconda3/lib/python3.8/site-packages/pysolar/solartime.py:110: UserWarning: I do
n't know about leap seconds after 2020
warnings.warn \
```

In [21]:

```
plt.scatter(times, Z)
plt.title("Angle solaire zénithal en fonction de l'heure d'acquisition (UTC)")
plt.grid()
```

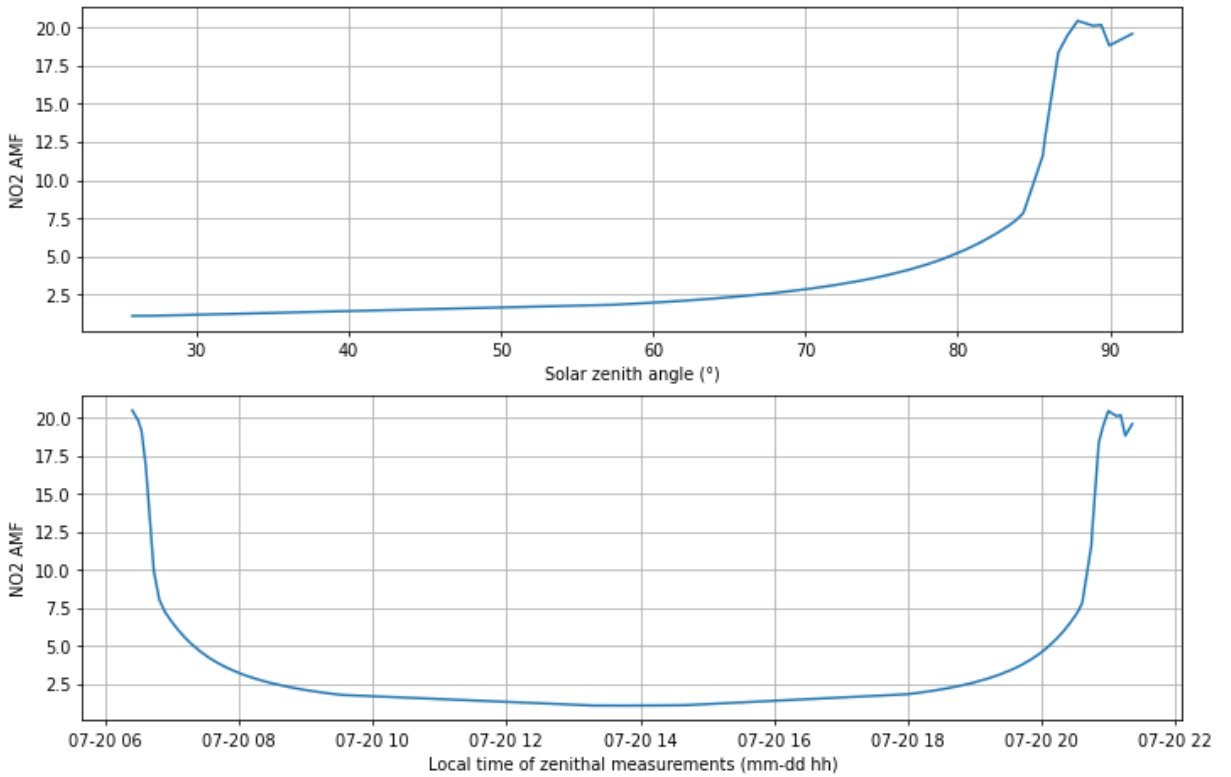
Angle solaire zénithal en fonction de l'heure d'acquisition (UTC)



In [22] :

```
_AMF = np.load('../processed/AMF.npy')
AMF = (np.cos(np.deg2rad(Z)) + .15*(93.885-Z)**(-1.253))**(-1)

plt.figure(figsize=(12,8))
plt.subplot(2,1,1)
plt.plot(Z[40:], _AMF[40:], label='AMF Sarki')
plt.xlabel('Solar zenith angle (°)')
plt.ylabel('NO2 AMF')
plt.grid()
plt.subplot(2,1,2)
plt.plot(localtimes, _AMF, label='AMF Sarki')
plt.xlabel('Local time of zenithal measurements (mm-dd hh)')
plt.ylabel('NO2 AMF')
plt.grid()
# plt.savefig('../report/img/amf-sarki.pdf')
# plt.legend();
```

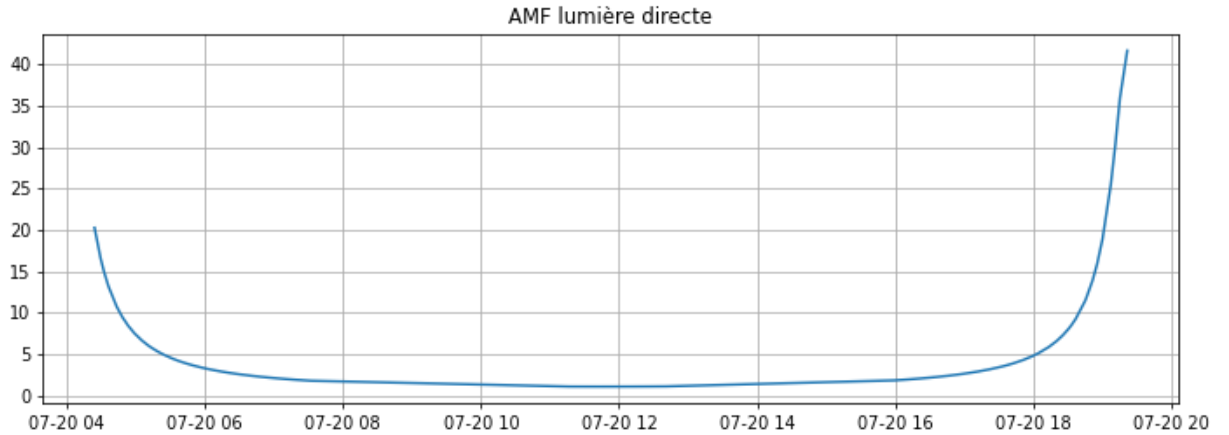


L'AMF obtenu avec le modèle de transfert radiatif de Sarki est incorrect aux angles solaires zénithaux proches de 90° et au-delà.

Nous choisissons l'AMF Sarki pour le lever ($Z < 88^\circ$) et l'AMF direct pour le coucher

In [23] :

```
plt.plot(times, AMF)
plt.title('AMF lumière directe')
plt.grid()
```

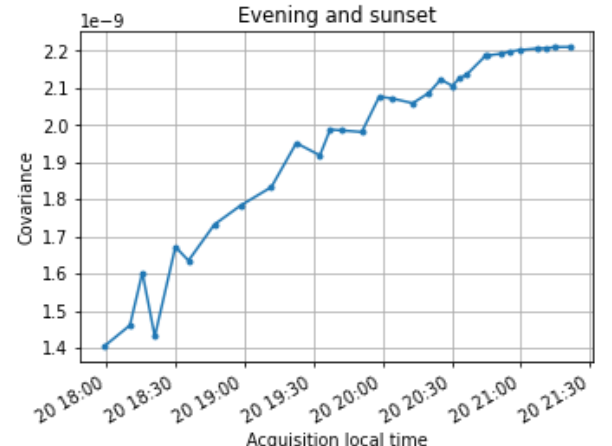
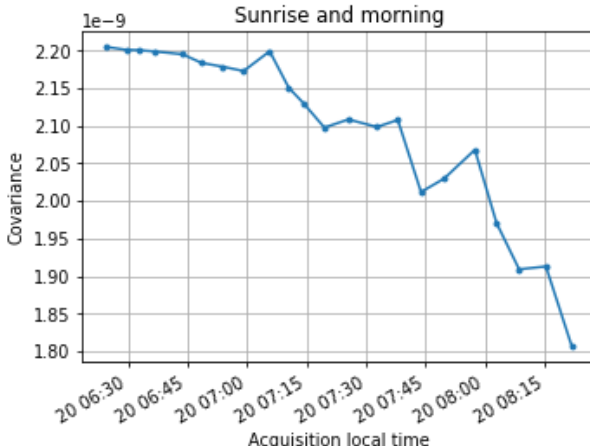


covariances en fonction des AMF

In [24] :

```
plt.figure(figsize=(12,4))
plt.subplot(1,2,1)
plt.plot(localtimes[:22], corrs[:22], marker='.')
# for i in range(15):
#     plt.text(_AMF[i], corrs[i], '{}'.format(i))
plt.title('Sunrise and morning')
plt.xlabel('Acquisition local time')
plt.ylabel('Covariance');
plt.grid()
plt.gcf().autofmt_xdate()

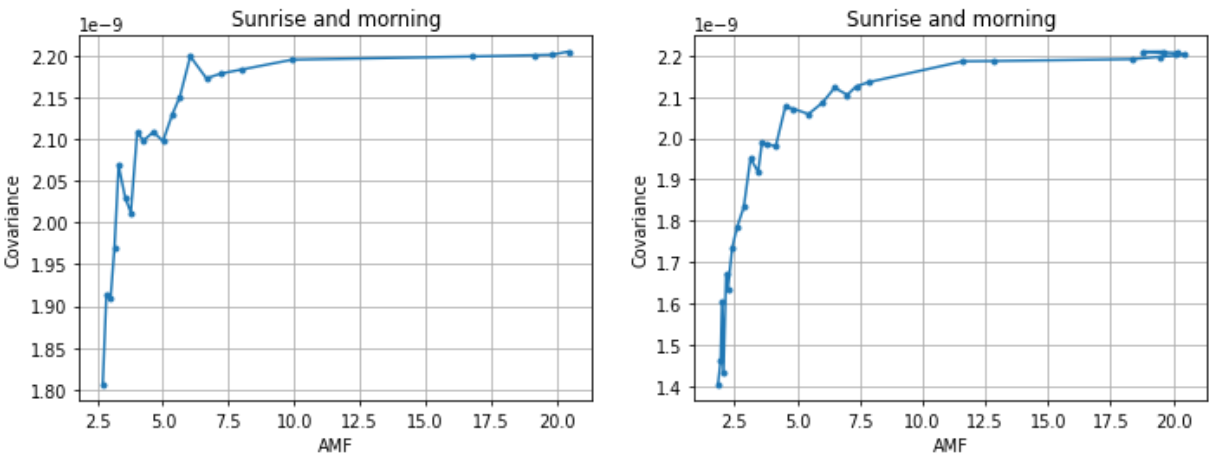
plt.subplot(1,2,2)
plt.plot(localtimes[43:], corrs[43:], marker='.')
# for i in range(15):
#     plt.text(_AMF[i], corrs[i], '{}'.format(i))
plt.title('Evening and sunset')
plt.xlabel('Acquisition local time')
plt.ylabel('Covariance');
plt.grid()
plt.gcf().autofmt_xdate()
#plt.savefig('../report/img/res-zenith-cov-zoom.pdf')
```



In [25] :

```
plt.figure(figsize=(12,4))
plt.subplot(1,2,1)
plt.plot(_AMF[:22], corrs[:22], marker='.')
# for i in range(15):
#     plt.text(_AMF[i], corrs[i], '{}'.format(i))
plt.title('Sunrise and morning')
plt.xlabel('AMF')
plt.ylabel('Covariance');
plt.grid()

plt.subplot(1,2,2)
plt.plot(_AMF[43:], corrs[43:], marker='.')
# for i in range(15):
#     plt.text(_AMF[i], corrs[i], '{}'.format(i))
plt.title('Sunrise and morning')
plt.xlabel('AMF')
plt.ylabel('Covariance');
plt.grid()
#plt.savefig('../report/img/res-zenith-cov-amf.pdf')
```

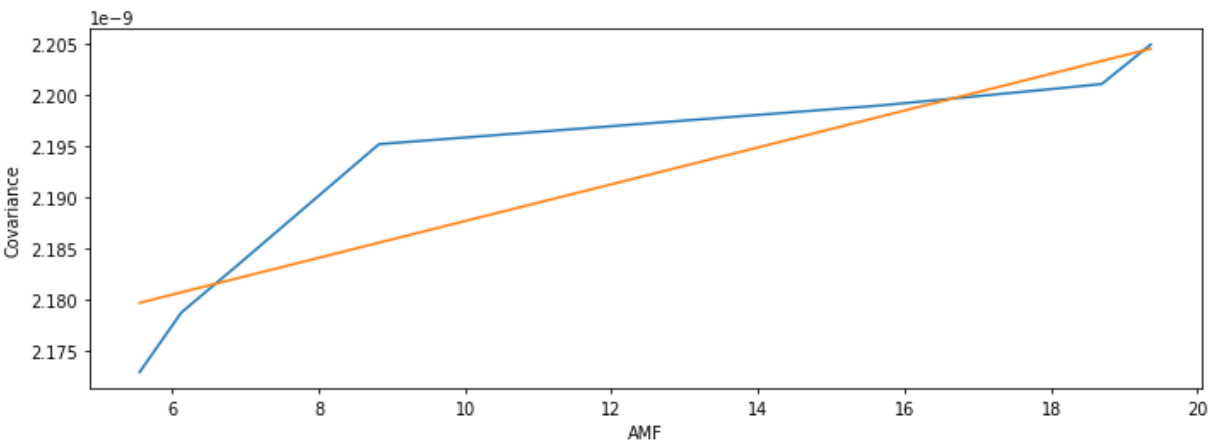


In [26] :

```
AMF_c, corrs_c = [amf - _AMF[40] for amf in _AMF[0:8]], corrs[0:8]
cov = np.cov(AMF_c, corrs_c)
b1 = cov[0,1]/cov[0,0]
b0 = np.mean(corrs_c) - b1*np.mean(AMF_c)
r2 = cov[0,1]**2/cov[0,0]/cov[1,1]
plt.plot(AMF_c, corrs_c)
plt.plot(AMF_c, b0+b1*np.array(AMF_c))
plt.title("covariance du matin\n"+
          "{} points\n".format(len(AMF_c))+
          "pente: {:.e} b: {:.e} r²: {:.2f}\n".format(b1, b0, r2))
plt.xlabel('AMF')
plt.ylabel('Covariance')

b1_matin = b1
vcd_matin_ohp = 3.4e15
```

covariance du matin
8 points
pente: 1.801610e-12 b: 2.169676e-09 r²: 0.85



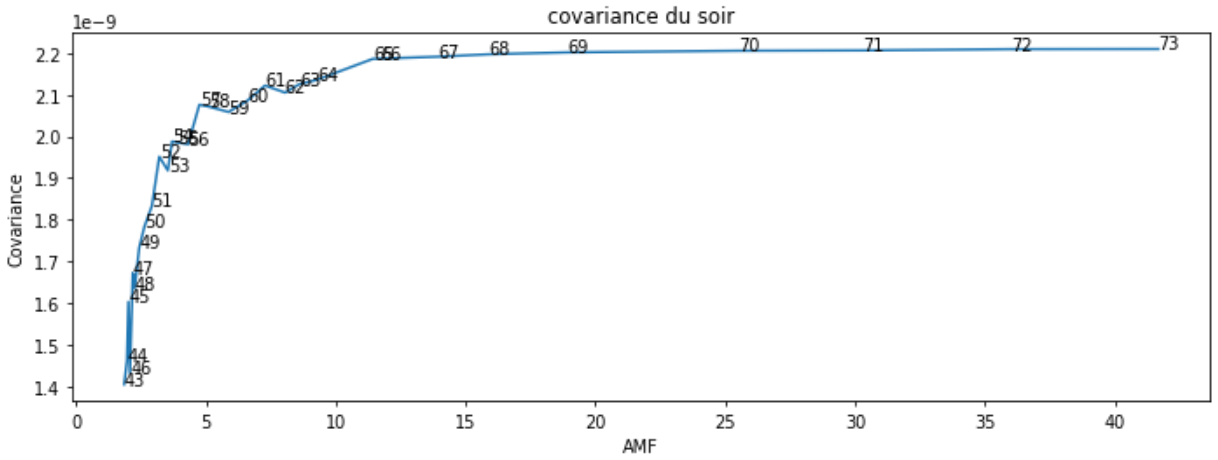
la pente est égale à $a \cdot \text{VCD}_{NO2\text{lever}}$ (voir plus haut)

en prenant pour référence $\text{VCD}_{NO2\text{lever}}$ donnée par les données mini SAOZ prises à l'OHP, on a $a = \text{pente} / \text{VCD}_{NO2\text{leverSAOZ}}$

on peut maintenant tenter d'estimer $\text{VCD}_{NO2\text{soir}}$ maintenant qu'on connaît a

In [27] :

```
plt.plot(AMF[43:], corrs[43:])
for i in range(43, len(AMF)):
    plt.text(AMF[i], corrs[i], '{}'.format(i))
plt.title('covariance du soir')
plt.xlabel('AMF')
plt.ylabel('Covariance');
# plt.ylim((0.95e-9, 1.05e-9))
# plt.ylim((3.8e-10, 4.15e-10))
```

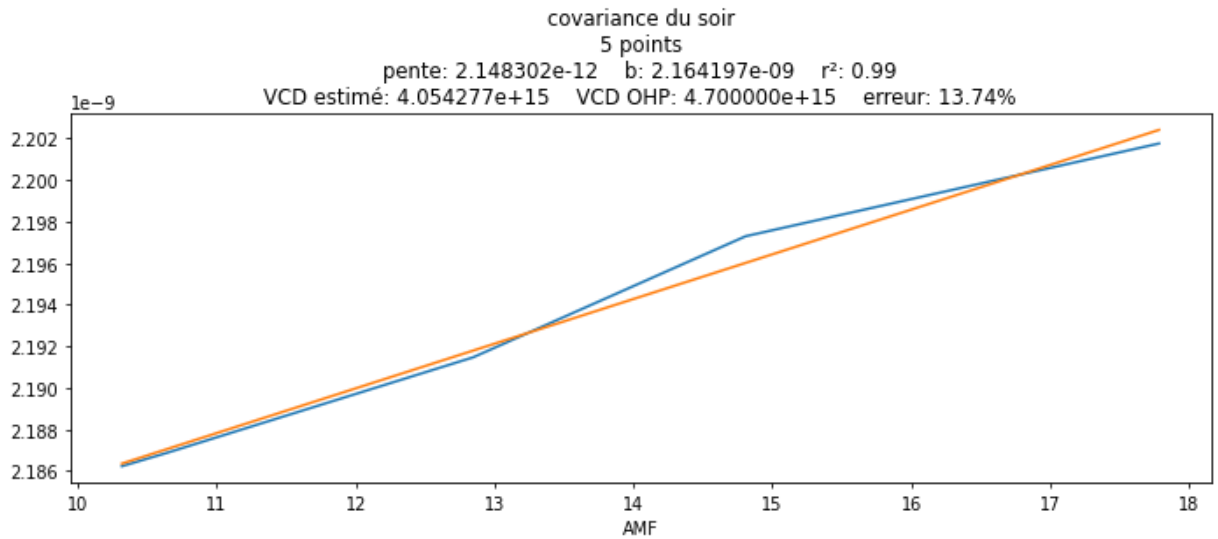


In [28]:

```
AMF_c, corrs_c = [amf - AMF[40] for amf in AMF[65:70]], corrs[65:70]
cov = np.cov(AMF_c, corrs_c)
b1 = cov[0,1]/cov[0,0]
b0 = np.mean(corrs_c) - b1*np.mean(AMF_c)
r2 = cov[0,1]**2/cov[0,0]/cov[1,1]

b1_soir = b1
vcd_soir = b1_soir * vcd_matin_ohp / b1_matin
vcd_soir_ohp = 4.7e15

plt.plot(AMF_c, corrs_c)
plt.plot(AMF_c, b0+b1*np.array(AMF_c))
plt.title("covariance du soir\n"+
          "{} points\n".format(len(AMF_c))+
          "pente: {} b: {} r²: {:.2f}\n".format(b1, b0, r2)+
          "VCD estimé: {} VCD OHP: {} erreur: {:.2f}%".format(vcd_soir, vcd_soir_ohp, 100*abs(vcd_soir-vcd_soir_ohp)/vcd_soir_ohp))
plt.xlabel('AMF')
```



Nous effectuons la régression linéaire dans la même zone d'AMF que pour les données du matin.